



Intelligent reflux and suction detection system for ventricular assist devices: in silico study

Bruno J. Santos^{1,2} · Idágene A. Cestari^{1,3}

Received: 1 January 2024 / Accepted: 26 November 2024 / Published online: 10 December 2024
© The Author(s), under exclusive licence to The Brazilian Society of Biomedical Engineering 2024

Abstract

Introduction Left ventricular assist devices (LVADs) serve both as a bridge to transplantation and as destination therapy for the treatment of congestive heart failure (CHF). However, the inability of the existing control strategies to automatically adapt LVAD flow according to hemodynamic changes can significantly impact patient survival and quality of life. Physiological control strategies for LVAD show promising results, with reflux and suction detection (RSD) increasing device safety.

Methods This study presents in silico results of an RSD system based on measurements of inlet and outlet pressures in continuous-flow LVAD. Two strategies were used to investigate control feasibility, safety, and adjustments to nonlinear variations and comprehensively assess the system's state considering a structured algorithm (SA) and ensembles of AI models (eAIM): K-nearest neighbors (KNN), support vector machine (SVM), and artificial neural network (ANN).

Results The SA submodule achieved an accuracy of 99.66% in suction detection but showed limitations in reflux events, with 80.04% accuracy and an F1-Score of 70.4%. The KNN and SVM models demonstrated performance exceeding 96% for both events, exhibiting more excellent stability than the SA submodule. The ANN excelled with low variability and an RMSE of 0.07 in R1, though its suction accuracy (96.7%) was slightly lower than for reflux (99.48%). The KNN was the most effective model, achieving 99.66% accuracy in suction and 98.44% in reflux. The SVM also produced competitive results but with variability across evaluations. The eAIM model showed satisfactory precision (97.78% for suction and 97.14% for reflux), with variations depending on the scenario. The eAIM is recommended for optimization in precision-critical situations.

Discussion These strategies are designed to fulfill the proposal's feasibility, flexibility, and safety requirements. They address the challenges of achieving consistent reproduction using an SA and the capability to handle nonlinear patterns. Additionally, they encompass the comprehensive assessment of the system's state through AI models and ensembles.

Conclusions This approach is unprecedented in identifying new waveform patterns to classify suction and reflux events and represents the first application of AI for integrating both adverse events, with improved robustness of results achieved through combining multiple AI models. The RSD system demonstrated excellent results, suggesting viability for application to PC-LVADs. The elevated results from the in silico study indicate only potential promise, with anticipated accuracy reduction in practical applications. Effective pattern detection in computational simulations highlights the need to assess the precision of the developed systems in in vitro and clinical studies.

Keywords Left ventricular assist devices (LVADs) · Physiological control · Backflow · Reflux · Suction · Structured algorithm programming · Artificial intelligence (AI)

✉ Bruno J. Santos
brunojsantos@usp.br

Idágene A. Cestari
idagene.cestari@incor.usp.br

¹ Biomedical Engineering Graduate Program, Polytechnic School of Engineering, University of São Paulo, Av. Prof. Luciano Gualberto, Travessa 3, nº380, São Paulo 05508-010, Brazil

² Department of Information Technology of Universidade São Judas Tadeu, Rua Taquari, nº546, São Paulo 03166-000, Brazil

³ Faculdade de Medicina, Bioengineering Division - Heart Institute, Hospital das Clínicas HCFMUSP, Universidade de São Paulo, LIM Bioengenharia, São Paulo, São Paulo, Brazil

Introduction

Heart failure (HF) is a major global health problem. Congestive HF (CHF) is the most debilitating stage, characterized by the heart's inability to pump enough blood to maintain a healthy life (Lilly 2022). While heart transplantation remains the gold standard for treating end-stage CHF, the limited number of available donors and potential contraindications limit its effectiveness (Mantha et al. 2022).

Left ventricular assist devices (LVADs) are used to prevent mortality in patients awaiting heart transplantation (bridge to transplant; BTT) and as destination therapy (DT) for those ineligible for transplantation (Goodman et al. 2022). Despite technological advances seen in the field with a significant reduction in adverse events (AEs) (Jorde et al. 2023), the long-term management of LVAD patients could be facilitated with improved LVAD controls. Commercial continuous flow LVADs (cfLVADs) typically operate at a fixed rate adjusted by clinicians during periodic visits according to the patient's need. Operation at a constant rate has limitations in response to changes in ventricular loads related to daily activities, posture, or emotional states (Stephens et al. 2020).

Physiological controls for LVADs (PC-LVADs) have been proposed to rapidly and automatically adjust the speed setpoint in response to demand and circulatory conditions (Stevens et al. 2018). Researchers in PC-LVADs have made progress in formulating control strategies (Santos and Leão 2021). However, this type of operation may lead to the generation of overpumping or underpumping (Tchantchaleishvili et al. 2017). To address this challenge, proposals for PC-LVADs incorporate a safety system against ventricular suction and reflux (also known as “backflow”) in the device (Pauls et al. 2016).

Vollkron et al. (2005) proposed a strategy to prevent reflux based on a predefined minimum speed. This approach is grounded in the premise that maintaining a minimum speed can mitigate the risk of reflux. However, this methodology may introduce a dead zone or a lower threshold that does not align with the individual patient's demand curve. Complementarily, in the study by Petrou et al. (2017), the concept of minimum flow is integrated as a lower threshold in the proportional-integral speed control. Adopting a strategy based on a predefined minimum value represents a straightforward approach that can effectively prevent reflux events in specific scenarios (Petrou et al. 2018). However, this may be inadequate for long-term support as it does not consider the particular physiological variations of each patient (Wu 2009).

In contrast, Leão et al. (2020) adopted a different approach based on artificial intelligence (AI). They

highlighted an automatic control component based on fuzzy logic, which regulates speed using heuristic rules to ensure a minimum safe flow. Similarly to the method proposed by Leão et al. (2020), recent research on PC-LVADs (Fetanat et al. 2021; Magkoutas et al. 2023) has implemented AI-based automatic control to overcome the limitations arising from the linearity of the control response and the intrinsic nonlinearity of natural physiological systems (Wu 2009). Despite promising results, the clinical application of this methodology is under rigorous evaluation due to concerns related to its robustness, particularly regarding the “interpretability/explainability” problem (de Sousa 2024) and challenges in integrating with commercial controllers (Santos et al. 2024).

Vollkron et al. (2005) proposed several safety strategies based on maintaining the flow signal's pulsatility index (Pindex) to prevent suction occurrence. This study calculates the Pindex for each cardiac cycle from the difference between the pump's maximum and minimum flow rates measured. Two other studies used the Pindex for the same purpose, although with different acquisition principles. In the study by Choi et al. (2007), the Pindex is derived from the cyclic variation of the hemodynamic load on the LVAD, using a flow estimator based on the LVAD motor's waveform. In the study by Petrou et al. (2017), the Pindex is based on the pressure wave measured by a pressure sensor in the inlet cannula. A more recent strategy for PC-LVADs based on Pindex was described by Melo et al. (2020), comprising a hierarchy of cascaded control loops that restored basal hemodynamic conditions under variations in systemic resistance and heart-beat rate, considering the specific physiological variations of each patient during assistance.

The suction prevention system proposed by Vollkron et al. (2005) gradually adjusts the speed when the Pindex falls below a predefined threshold, applied by other authors (Choi et al. 2007; Wang et al. 2015; Petrou et al. 2017) using a flow sensor. A real-time ultrasonic flow sensor is used in the outflow cannula of the HeartAssist5 and aVAD (Reliant-Heart Inc., Houston, TX, USA) (Deniz et al. 2017). Despite the success of this approach, the accuracy of flow measurement was questioned in a clinical trial of this LVAD, where a consistent discrepancy of 24–29% was found between the flow probe and the cardiac output measured by a Swan-Ganz catheter (Sayer et al. 2017). The technical challenges associated with designing and implementing devices capable of providing continuous postoperative cardiac volume information using soft, flexible sensors made of biocompatible materials implanted on the heart surface are well-documented (Dual et al. 2020).

In this context, alternatives have been advocated in the literature, such as using estimators based on pump motor waveforms (Horvath et al. 2018) and pressure sensors (Ishii et al. 2012). However, the use of sensorless estimators can be

inaccurate in a clinical context or entirely unfeasible when there are changes in pump characteristics or device motor types (Pauls et al. 2016; Petrou et al. 2018), while the use of pressure sensors faces criticism for decreased sensitivity over time and sensor drift (Tchantchaleishvili et al. 2017). This view is being challenged by new proposals for PC-LVAD designs resistant to drift (Petrou et al. 2016) and reliable long-term sensors (Petersdorff-Campen et al. 2021). Additionally, a recent study highlighted the superiority of sensor data in ensuring the proper functioning of PC-LVADs (Santos and Cestari 2023).

Vollkron et al. (2005) proposed a strategy centered on maintaining the Pindex of the flow signal to prevent suction. However, this approach necessitates a flow sensor, which is impractical for implantable clinical settings. In response, Petrou et al. (2017) introduced a Pindex that utilizes a pressure sensor. This study presents a reflux and suction detection (RSD) system that employs a pressure sensor and computational simulations to identify critical points and optimize thresholds within a structured algorithmic submodule for detecting suction events. Both Vollkron et al. (2005) and Petrou et al. (2017) methods do not account for reflux events during support; instead, a constant minimum value is employed to mitigate the risk of reflux. Although this method is practical, it has been criticized for lacking generalizability, resulting in suboptimal thresholds. Consequently, the RSD system adopts a strategy similar to suction detection, investigating additional points of interest and adjusting contour thresholds within the structured algorithmic submodule to detect reflux during support.

The RSD structured algorithmic submodule aims to be a simple code suitable for integration into commercially available microcontroller-based controllers (Santos et al. 2024). An AI-based submodule of the RSD was designed to address nonlinear patterns, utilizing training data obtained from a Computational Simulator of PC-LVADs (CS-PC-LVADs) with CHF patient models. Furthermore, an ensemble of AI models was implemented to increase confidence in the performance of AI model results that meet Health 4.0 criteria (Santos et al. 2023).

The strategies employed to develop the RSD system submodules include (i) a structured algorithm and (ii) an ensemble of AI models. The division into submodules is justified by enhancing safety through a system with redundancy in identifying AE and the occurrence of suction and reflux. The RSD system proposed in this study presents novel methodologies based on pressure wave analysis. This approach is novel as it identifies new waveform patterns for classifying suction and reflux events. It represents the first application of AI for this purpose, with enhanced robustness of results achieved through integrating multiple AI models.

The manuscript is organized with an “Introduction” in Section 1, followed by a presentation of “Methods” in

Section 2. This section provides a comprehensive overview of the design and in silico evaluation, highlighting the key components integral to the proposed system’s development. The “Results” section presents the results discussed in “Discussion” section, followed by “Conclusions” in Section 5.

Methods

The flowchart in Fig. 1 outlines all the steps involved in formulating and validating the RSD system’s submodules. It was developed to clarify the methods used in this proposal. The flowchart represents each process stage using distinct symbols and colors: purple denotes data input, blue represents processing, yellow indicates decision-conditions, and red signifies data storage. Arrows in the flowchart show the progression between steps. In the following sections, each flowchart component will be examined in depth.

The data for formulating and validating the RSD system’s submodule were procured from a computational simulator of PC-LVADs (CS-PC-LVADs) incorporating models of patients with CHF. The CS-PC-LVADs is a module previously described (Santos and Cestari 2024) and integrated into a previously described automated simulator of systemic circulation (Torres et al. 2021); its objective is to be used for comparative analysis of hemodynamic responses in a simulated patient equipped with an LVAD. The described CS-PC-LVADs include (i) simulations of the physiological state of the patient, (ii) mathematical models of estimators and sensors, and (iii) PC-LVAD algorithms.

The CS-PC-LVADs use LabVIEW software (V.2018, National Instruments, Austin, USA) and integrate the Harvi platform (PVLoops LLC, Baltimore, USA) to simulate the patient’s physiological parameters (Bouchez et al. 2023). Based on electrical systems, the cardiovascular model represents the circulatory system and allows real-time simulation of hemodynamic behavior (Bronicki et al. 2022). This allows analytical and graphical expressions of pressure-flow relationships at different locations within the model (Doshi and Burkhoff 2016).

Drift-free calibrated pressure sensor models are used and incorporated into the cannulae to track changes in the patient’s cardiac status within the CS-PC LVADs. At the same time, estimators based on a look-up table (LUT) technique are applied to the centrifugal pump. These operational blocks are integrated using interpolation techniques to represent physiological behavior and cfLVAD variables across operational regions.

The patient was represented by a simulated mathematical model within the Harvi platform, which includes a centrifugal cfLVAD model analogous to the HeartMate3 (Peev and Salerno 2023). This device was implanted between the inlet cannula at the apex of the left ventricle and the outlet

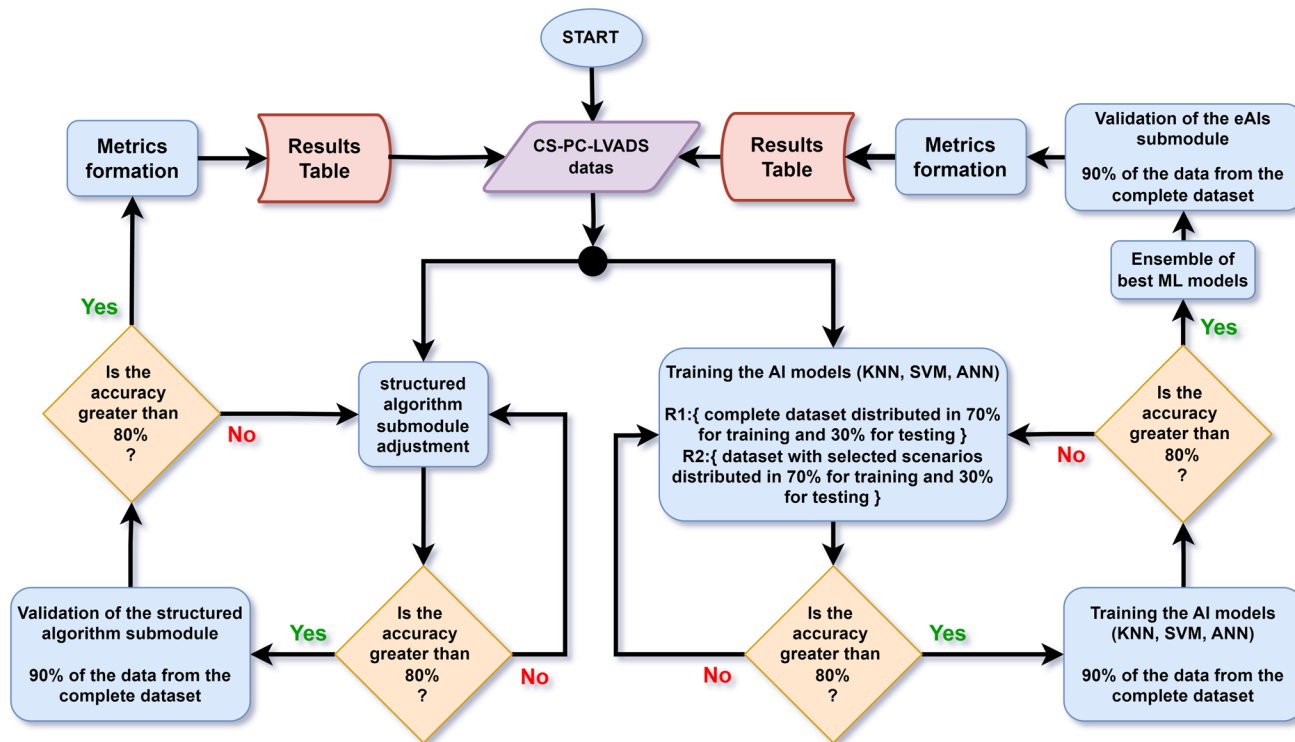


Fig. 1 Flowchart of the formulation and validation process for the RSD system's submodule. The flowchart depicts the process steps, using different colors to represent data input (purple), processing (blue), decision-conditional (yellow), and data storage (red), with

arrows indicating the sequence between stages. CS-PC-LVADS computational simulator of physiological controls for left ventricular assist devices, R1 round 1, R2 round 2

cannula in the aortic artery. The 27 scenarios considered were derived from three primary parameters: HR, preload, and afterload. A summary of the characteristics of each scenario is presented below:

Scenarios 1 to 9: Maintain a constant afterload of 8.5 mmHg*min/L, varying the HR between 60, 90, and 120 bpm, and the preload between 2200 ml, 2500 ml, and 2700 ml.

Scenarios 10 to 18: Increase the afterload to 18.5 mmHg*min/L, maintaining the same variations in HR and preload as the previous scenarios.

Scenarios 19 to 27: Elevate the afterload to 32 mmHg*min/L, following the same pattern of variation as the previous two groups.

This structuring allowed for analyzing the isolated impact of varying these parameters on the cardiovascular system while keeping the others constant. For instance, scenarios 1, 4, and 7 enable observing the effects of altering preload with a constant HR of 60 bpm and a constant afterload. Similarly, scenarios 1, 10, and 19 facilitate understanding the impact of increasing afterload with constant HR and preload.

Simulated patient data in CS-PC-LVAD considering a range of physiological conditions representative of various CHF stages and activity levels, aiming to minimize the impact of the reported linear model issue. The selection of the values for the three primary parameters is based on the methodology that Magkoutas et al. (2023) proposed to optimize the physiological control parameters of cfLVADs.

For each of the 27 physiological variation scenarios, the cfLVAD speed was adjusted from 3000 to 9000 rpm in increments of 100 rpm. Data was simulated and stored via output recordings with an entire waveform represented by 200 measurement points (0 to 1000 s in 5 s increments) containing information on left ventricular (LV) pressure (used as LVAD input pressure; mmHg), LVAD differential pressure (mmHg), output pressure (calculated by adding LVAD differential pressure and LV pressure; mmHg), LVAD flow (L/min) used to identify reflux by the negative value, and LV suction status (true or false).

RSD system development

A detailed flowchart in Fig. 2 was developed to describe all the steps involved in the operation of the RSD system, aiming to clarify the proposal's functioning. The flowchart

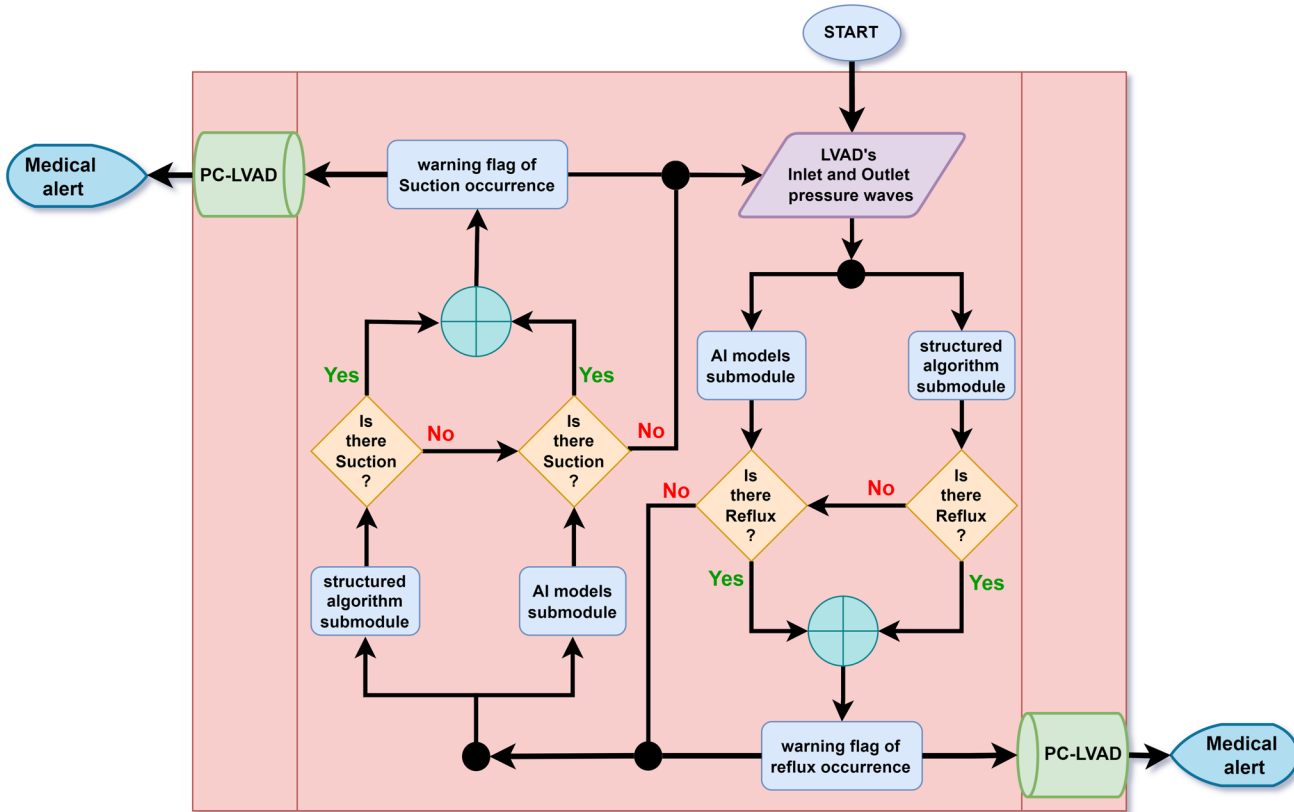


Fig. 2 Flowchart of the operational stages for the RSD system submodule, using color codes to represent data input (purple), processing (blue), decision-conditions (yellow), logical “OR” (light blue), PC-LVAD connection (green), and medical device display (dark blue).

Arrows indicate the sequence, with the entire diagram framed in pink to denote its module integration with the PC-LVAD system. *LVADs* left ventricular assist devices, *PC-LVAD* physiological controls for LVAD

illustrates each process stage using distinct symbols and colors: purple represents data input, blue denotes processing, yellow indicates decision-conditions, and light blue signifies “OR” logic. Green means connecting to the PC-LVAD, while dark blue corresponds to information displayed on a medical device. Arrows in the flowchart indicate the progression between stages. The entire flowchart is enclosed in a pink rectangle, highlighting that it constitutes an integrated module of the PC-LVAD system.

In the following sections, each submodule of the RSD system will be thoroughly examined, and the approaches for developing the strategies for these submodules will be presented: “RSD system: structured algorithm (SA) submodule,” “RSD system: ensemble of AI models (eAIM) submodule.”

RSD system: structured algorithm submodule

Classifying suction and return events using pressure wave data presents a significant mathematical problem. A prevalent strategy to tackle such mathematical complexities involves using algorithms adhering to structured

programming principles (Dahl et al. 1972). These principles encompass sequence, selection, and iteration methodologies.

The structured algorithm (SA) submodule of the RSD system was based on the premise that suction and reflux states could be detected by morphological changes in the pressure wave captured by sensors in the cannulae. The goal was to find ideal thresholds representing an optimal classification range without significantly reducing the control ranges in certain situations. The dataset was extensively analyzed to identify patterns that could serve as state conditions in the structured algorithm and met two critical criteria: feasibility for implementing microcontrollers widely used in commercial LVAD controllers and the ability to deal with physiological variations.

According to the literature, suction has an easily identified pattern (Vollkron et al. 2005; Choi et al. 2007; Petrou et al. 2017). A reduction in Pindex is caused by the absence of additional flow in the ventricle during contraction. As a result, there is no extra fluid entering the device, and there is no relationship between two peaks: the nominal pumping of the device and the additional blood entry due to the contraction of the native heart. As shown in Fig. 3, there is

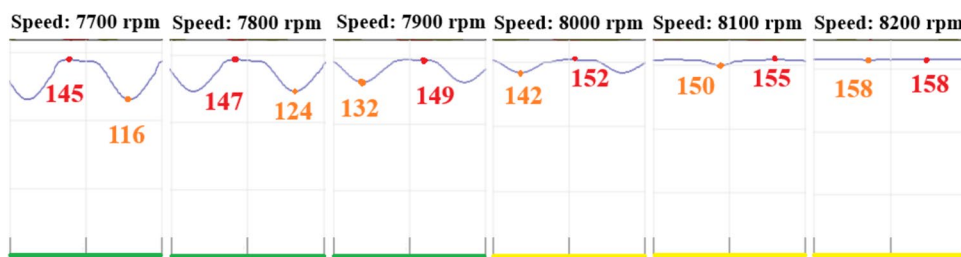


Fig. 3 A comparison of the left ventricular pressure waveform for selected speeds illustrates the transition between the non-suction state (highlighted in green) and the suction state (highlighted in yellow),

a decrease in the Pindex of the cfLVAD differential pressure as the speed increases and suction is initiated (highlighted in yellow).

No specific pattern has been reported in the literature to identify reflux. Results of simulations performed in this study show that as the reflux state becomes apparent, additional sawtooth waveforms are observed with a separation between the maximum and intermediate peaks. Additionally, there is an increase in the depth of the representative value within the region of minimum pressure during the diastolic phase of the heart, as illustrated in Fig. 4. This additional sawtooth wave and the associated deepening of the trough related to the opposing signal component may be linked to the presence of aortic pressure wave elements within the LV pressure wave. This phenomenon occurs because the cfLVAD acts almost like an open bridge between the ventricle and the artery at low speed and, consequently, low fluidic resistance.

The SA submodule of the RSD system proposes an approach based on points of interest and boundary limits to identify AEs, such as ventricular suction and reflux. In this context, two pressure waves obtained during the same cardiac cycle are compared: one during normal assistance and the other during the AE occurrence of suction or reflux. The goal is to identify distinguishing features that can serve as decision criteria. The R2 dataset was selected as the reference basis for the pressure waves for three reasons: (i) the

with a noticeable reduction in the difference between the maximum and minimum values

R1 dataset is enormous for this type of analysis, requiring complex techniques such as nonlinear fitting or decision tree algorithms. Although these techniques are viable, they do not align to make the SA submodule easily adjustable and implementable in simple embedded systems; (ii) the R2 dataset was explicitly constructed to capture initial scenarios without the occurrence of suction or reflux and final scenarios with the occurrence of these events, complemented by the states immediately preceding and following such events, making it ideal for the purpose without compromising system performance; (iii) due to the antagonistic operation of the pump speed, which can cause reflux (at low speeds) or ventricular suction (at high speeds), there is no simultaneity between these events. Their logic is mutually exclusive (when one is true, the other must necessarily be false).

The predictor variables of the R2 dataset were presented in graphs (Fig. 5), consolidating information about the inlet cannula pressure, outlet cannula pressure, and the differential pressure between them, considering 27 physiological variations. The organization of the graphs is as follows: (A) initial state of suction detected as false/final state of reflux detected as true, in various simulated scenarios; (B) state of suction detected as false, in various simulated scenarios; (C) state of suction detected as true, in different simulated scenarios; (D) final state of suction detected as true/initial state of reflux detected as false, in different simulations; (E) state of reflux detected as false; (F) state of reflux detected as true,

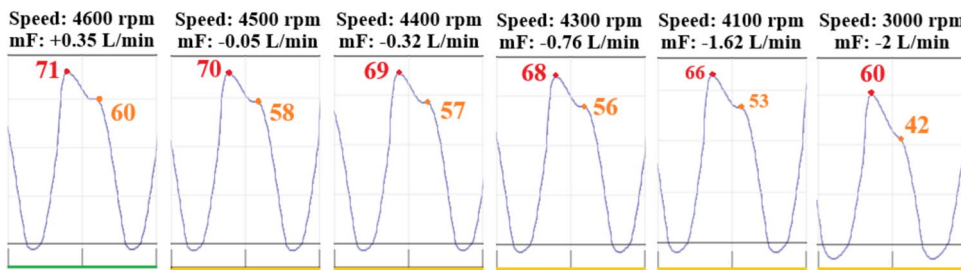


Fig. 4 Comparison of the left ventricular pressure waveform for selected velocities to illustrate the transition between the non-reflux state (highlighted in green) and the reflux state (highlighted in yellow),

where a noticeable increase in the difference between the maximum and mean values, along with the formation of an additional sawtooth wave, can be seen. *mF* minimum flow

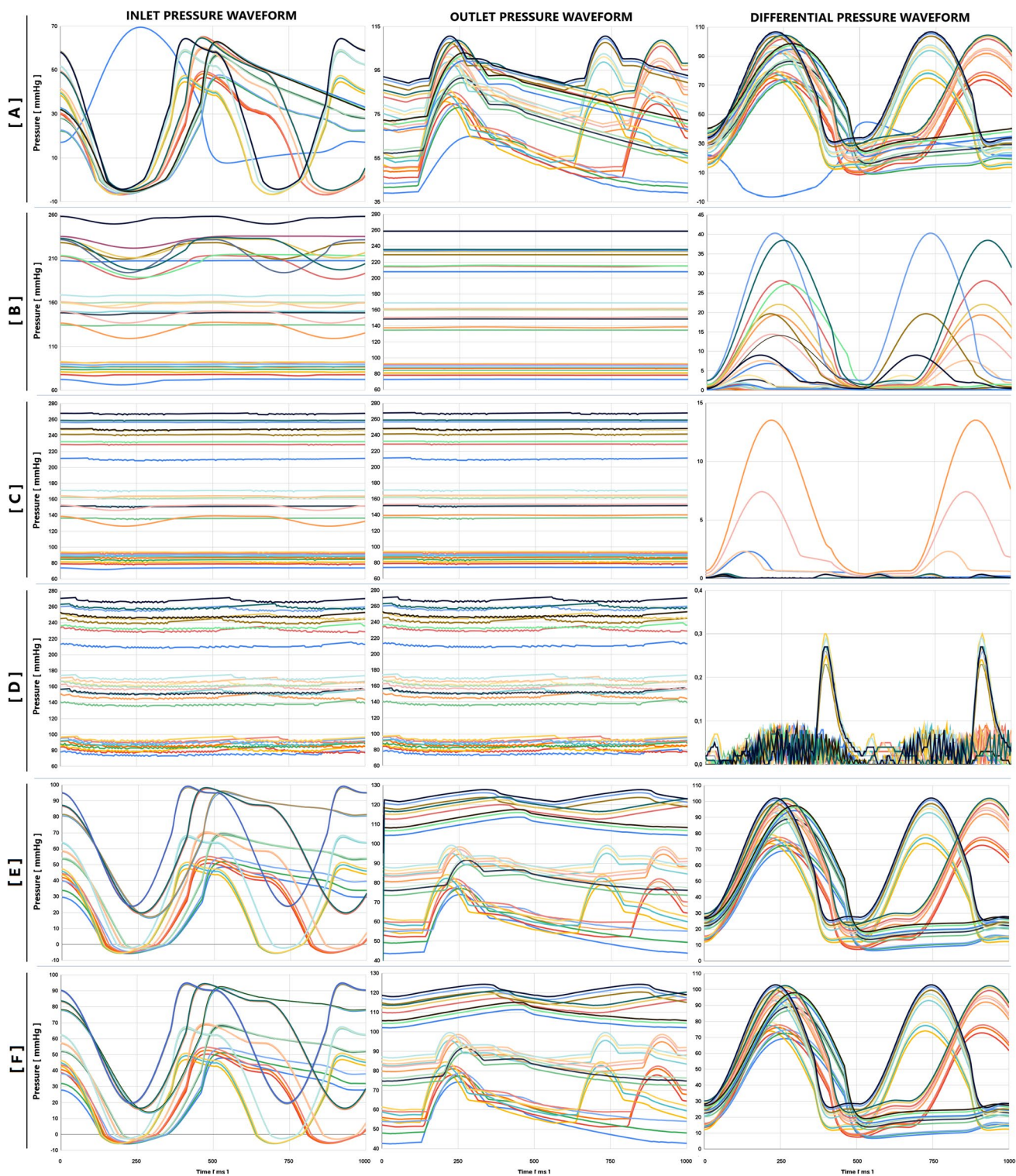


Fig. 5 Pressure waveforms for inlet, outlet, and differential pressures from the R2 dataset illustrate 27 physiological variations across multiple simulated scenarios. The plots are organized as follows: **A** initial state of suction identified as false and final state of reflux identified as

true; **B** state of suction identified as false; **C** state of suction identified as true; **D** final state of suction identified as true and initial state of reflux identified as false; **E** state of reflux identified as false; **F** state of reflux identified as true

both in various simulated scenarios. A vital note refers to the blue line in graph A, representing a situation in which the LVAD pump is almost “off” (minimum speed), simulating a healthy patient (scenario 1: heart rate of 60 bpm, preload of 2200 ml, and afterload of 8.5 mmHg min/L). This graph serves as a reference, as the pressure reflected corresponds to that of a healthy patient with minimal assistance, differing from the other scenarios.

The method used to identify points of interest in the pressure waves to assist in classifying adverse events followed this procedure: first, the three pressure wave sources (inlet cannula, outlet cannula, and differential pressure between them) were analyzed for all physiological variations. Then, a reference value was established. In the initial state (without the occurrence of adverse events; Fig. 5A for the suction event and Fig. 5D for the reflux event), all waves above this value were classified as safe, with no indication of critical events (reflux or suction). In the final state (with the occurrence of adverse events; Fig. 5A for the reflux event and

Fig. 5D for the suction event), all waves below this value were classified as indicative of critical events. Finally, it was verified whether this value provided a clear transition in the classification of AEs in the waves immediately before (Fig. 5B for the suction event and Fig. 5E for the reflux event) and after (Fig. 5C for the suction event and Fig. 5F for the reflux event) an AE.

This method identified a point of interest (A1) in the differential pressure wave used to classify suction events, as illustrated in Fig. 6. This point’s amplitude is 0.25 mmHg, and its morphological location occurs during the ascending phase of the wave, representing the positive rate of change in the differential pressure between the inlet and outlet of the LVAD throughout the cardiac cycle. As illustrated in Fig. 3, when a ventricular suction event occurs, the inlet and outlet pressures become closely approximated, and the differential pulsatility is reduced to a significantly lower level.

Similarly, a point of interest (B1) was identified in the inlet cannula pressure wave, used to classify reflux events,

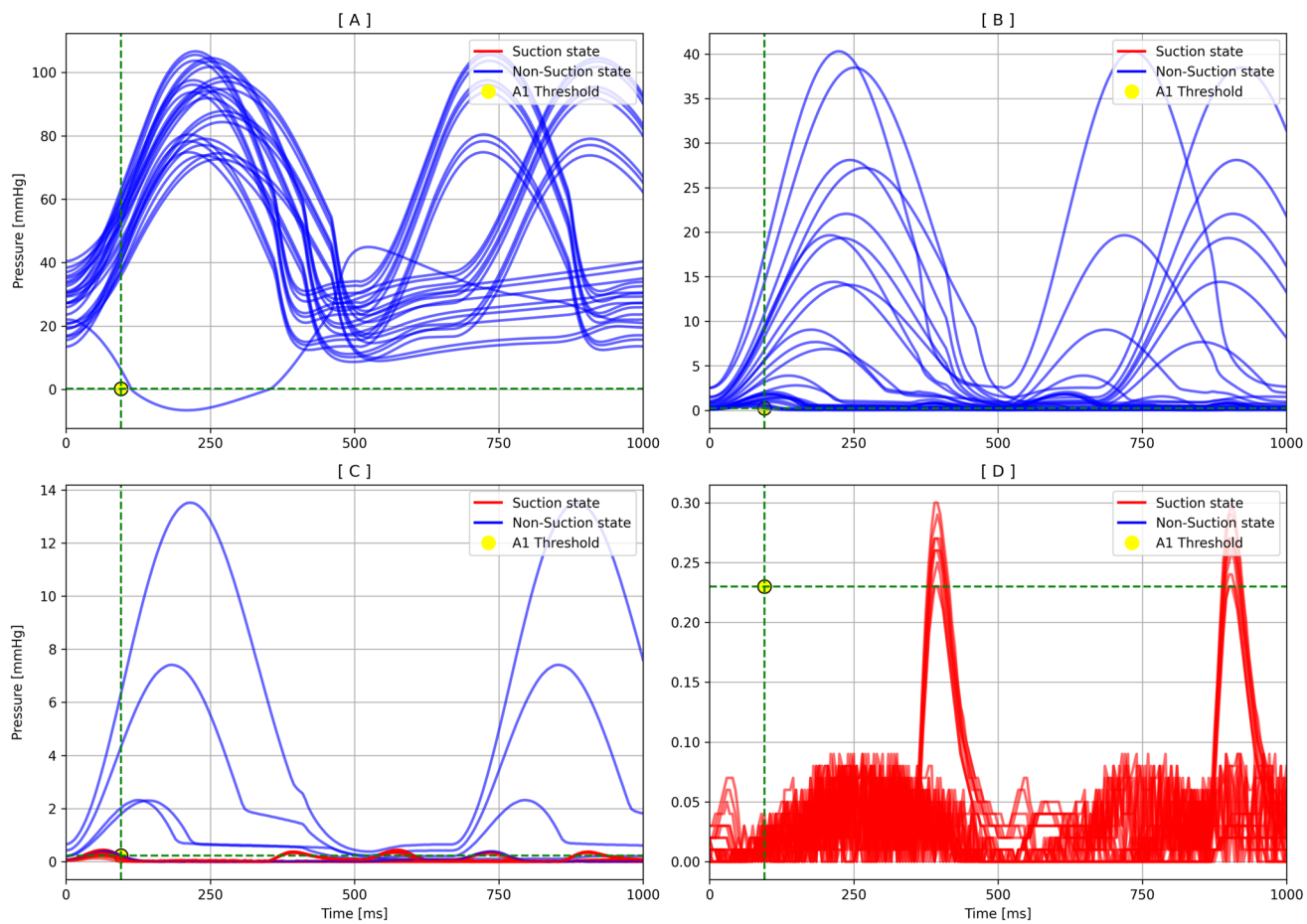


Fig. 6 Differential pressure waveform plots between the cfLVAD inlet and outlet cannulae were generated to illustrate the morphological changes observed between the non-suction state (highlighted in blue) and the suction state (highlighted in red) in 27 physiologi-

cal variations across multiple simulated scenarios. The graphs present selected points of interest (A1) critical for assessing the transition between standard support and suction states

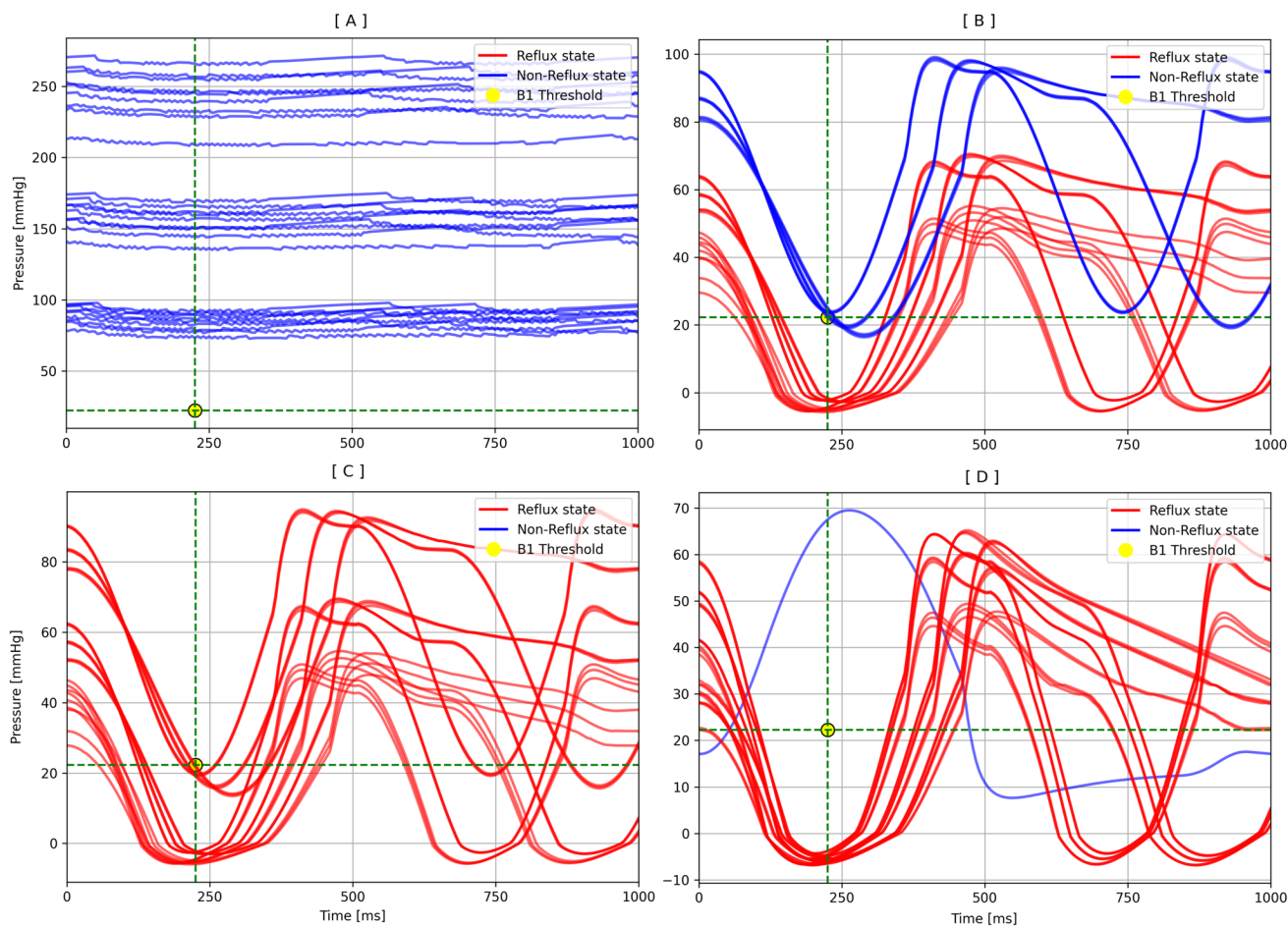


Fig. 7 Inlet pressure waveform plots of the cfLVAD illustrate the morphological changes observed between the non-reflux state (highlighted in blue) and the reflux state (highlighted in red) across 27

physiological variations in multiple simulated scenarios. The graphs also present selected points of interest (B1) critical for assessing the transition between standard support and reflux states

as illustrated in Fig. 7. This point's amplitude is 22 mmHg, and its morphological position occurs at the trough of the pressure wave, representing approximately the minimum diastolic pressure value during the cardiac cycle. As identified in the pattern shown in Fig. 4, during the reflux event, a sawtooth formation appears in the composition of the incoming pressure wave, deepening the trough region. This indicates increased pressure in the opposite direction of the pumping flow.

Thus, the SA submodule of the RSD system can be described as follows: (i) if the differential pressure wave value is less than or equal to 0.25 mmHg, considering the average value \pm a standard deviation of 2 mmHg during the ascending phase of the differential pressure wave, there is an indication of ventricular suction; (ii) if the inlet cannula pressure wave value is less than or equal to 22 mmHg, considering the average of the minimum pressure value \pm a standard deviation of 2 mmHg, there is an indication of reflux in the device.

RSD system: an ensemble of AI models submodule

The AI approaches discussed in the literature (Fetanat et al. 2021; Magkoutas et al. 2023) have been extended to include other AI models in this version of the RSD system.

The method for detecting suction and reflux in the LVAD using AI models involves the following five steps: (i) creation of a dataset; (ii) preprocessing of the dataset; (iii) selection of AI models; (iv) training of AI models; and (v) evaluation of the performance of each AI model.

The dataset generation (step 1) was based on 27 physiological variation scenarios, with the cfLVAD speed adjusted from 3000 to 9000 rpm in increments of 100 rpm for each scenario obtained in the CS-PC-LVAD. This resulted in a total of 1647 data rows.

In the preprocessing phase (step 2), the dataset was organized into 605 columns based on 201 columns representing the differential pressure variation in a complete waveform, an additional 201 columns for the input pressure variation

in a complete waveform, and another 201 columns for the output pressure variation in a complete waveform. In addition, a suction state column was added with data values of 0 or 1 based on the suction status of the left ventricle. Finally, a reflux state column was added with data values of 0 or 1 based on negative values in the LVAD minimum flow.

The AI model selection (step 3) was based on the representation of the main niches of mathematical model architectures: K-nearest neighbors (KNN) identifies similarities between received patterns and those in the training dataset, influencing classification based on the nearest patterns (Zhang 2016); support vector machine (SVM) constructs a hyperplane to separate different patterns, with support vectors crucial for classification (Cervantes et al. 2020); and artificial neural network (ANN), composed of interconnected neurons, excels in capturing complex relationships and temporal patterns, automatically extracting hierarchical features, and adapting to different patterns (Abiodun et al. 2018).

These AI models were selected as representatives of AIs with similar characteristics, such as SVM and linear regression. The models were trained on the same training data and exhibited different features and learning capabilities. The sci-kit-learn library (<https://scikit-learn.org/stable/>), widely recognized in the machine learning and deep learning community, was developed in Python to implement the basic AI models.

The Grid Search technique was employed to identify the optimal hyperparameters for the ML models. This method systematically evaluates all possible combinations of pre-defined hyperparameters within a search space. Hyperparameters, which govern algorithm behavior without being directly learned from the data, are crucial for model performance. Grid Search ensures robust hyperparameter selection by employing cross-validation, which mitigates overfitting and enhances generalization.

Cross-validation is a fundamental technique to assess a model's generalization ability to unseen data. This approach divides the dataset into multiple subsets or folds, and the model is iteratively trained and tested on distinct partitions. In k-fold cross-validation, the data is split into k equal parts. In each iteration, one fold is reserved for testing, while the remaining $k - 1$ folds are used for training. After completing k iterations, the performance metrics (e.g., accuracy or mean squared error) are averaged to provide a reliable estimate of the model's predictive capabilities.

The following hyperparameters were configured for the KNN algorithm:

- n_neighbors: Defines the number of neighbors considered during classification or regression. A smaller value (e.g., 1) may lead to overfitting, while larger values

increase bias by smoothing decision boundaries. Typical starting values range between 3 and 7.

- Weights: Specifies how neighbors influence predictions. If set to "uniform," all neighbors contribute equally. If set to "distance," closer neighbors are given more weight, which benefits datasets with uneven distributions.
- Algorithm: Defines the strategy used to search for neighbors, with options including "ball_tree," "kd_tree," or "brute." Tree-based methods offer efficiency for large datasets, while brute-force search provides exhaustive results at a higher computational cost.
- Leaf_size: Controls the maximum size of leaf nodes in tree-based algorithms. Smaller leaves reduce query time but increase the time needed to build the tree, while larger leaves expedite tree construction at the expense of slower queries.
- Metric: Specifies the distance function used to compare data points. The default metric is the Minkowski distance, where the parameter p adjusts the distance type: $p=1$ corresponds to the Manhattan distance, and $p=2$ corresponds to the Euclidean distance. Selecting the appropriate metric is critical for achieving optimal model performance.

For the SVM algorithm, the following hyperparameters were configured:

- C parameter: Balances the trade-off between maximizing the margin and minimizing classification errors. Higher values of C impose stricter penalties for misclassifications, potentially leading to overfitting, while lower values allow more margin violations, enhancing generalization. A recommended starting point is $C = 1.0$.
- Kernel function: Maps the data to higher-dimensional spaces to handle complex decision boundaries. The "linear" kernel is adequate for linearly separable data, while the "poly" (polynomial) and "rbf" (radial basis function) kernels are better suited for nonlinear cases. The "sigmoid" kernel emulates the activation functions used in neural networks. The degree parameter controls complexity for polynomial kernels, with higher degrees capturing more intricate patterns.
- Gamma parameter: This parameter determines the influence of individual data points on the decision boundary. With "scale," gamma is set based on the variance of the input data, while "auto" sets it to the inverse of the number of features. Higher gamma values create more localized decision boundaries, while lower values produce smoother regions.
- coef0 parameter: Applies to polynomial and sigmoid kernels, controlling the impact of the independent term in the decision function. It does not affect the RBF kernel.

- Shrinking heuristic: Enhances computational efficiency without compromising accuracy, particularly for large datasets.
- Probability parameter: When enabled, the model provides class probabilities during prediction, albeit at the cost of additional computation.

For the ANN, the following hyperparameters were defined:

- Hidden_layer_sizes: This specifies the network's architecture by defining the number and size of hidden layers. For instance, (100) creates a single hidden layer with 100 neurons. Deeper architectures capture more complex patterns but may increase overfitting risks and computational demands.
- Activation function: Defines how inputs are transformed within each neuron. Standard options include “identity” (no transformation), “logistic” (sigmoid function), “tanh” (hyperbolic tangent), and “relu” (rectified linear unit). ReLU is favored for its computational efficiency and ability to mitigate the vanishing gradient problem during backpropagation.
- Solver: Refers to the optimization algorithm used for training. Popular solvers include “lbfgs” (a quasi-Newton method), “sgd” (stochastic gradient descent), and “adam” (adaptive moment estimation). Adam is often preferred for its fast convergence and robustness across various datasets.
- Alpha parameter: Regulates L2 regularization, which penalizes large weights to reduce overfitting risks.
- Batch size: Determines the number of samples processed per iteration. Smaller batch sizes offer higher precision but increase training time.
- Learning rate: Controlled via the learning_rate_init parameter, which defines the initial learning rate of the optimizer. High learning rates can impede convergence, while meager rates slow the training process.
- Max iterations: The max_iter parameter sets the maximum number of training iterations. Increasing this value may be necessary when learning progresses slowly, though it will prolong training time.

The datasets utilized for training and testing (step 4) comprise two distinct rounds: Round 1 (R1) and Round 2 (R2). The R1 dataset for training and testing consists of 27 physiological variations, resulting in a dataset with 1647 rows and 605 columns. The R2 dataset for training and testing also consists of 27 physiological variations, focusing on specific scenarios, including the initial state with no reflux/suction occurrence and the final state with reflux/suction occurrence. Additionally, the states were selected

immediately before and after a reflux/suction event, forming a dataset with 109 rows and 605 columns.

The R1 and R2 datasets were divided into 70% for training and 30% for testing, a widely accepted method that effectively reduces the risk of overfitting. During the training phase, each AI model underwent 2000 extended training epochs, lasting approximately 1 h, utilizing the same dataset for consistency in model development. Extensive preprocessing steps were carried out, including normalization and balancing of values. Based on these analyses, no bias or dependencies within the dataset were detected.

The initial phase of the training process involves using accuracy as a criterion to determine the model's progression, with a minimum threshold set at 80%. If the model achieves this accuracy level during training, it advances to the validation stage, where accuracy is reassessed. If the model's performance remains above 80%, it is saved; otherwise, it is returned to the training phase for further adjustments. This evaluation cycle ensures continuous model optimization before the final performance metrics assessment.

The second submodule of the RSD system encompasses the most optimized versions of the previously discussed AI models—namely KNN, SVM, and ANN—which were selected based on their superior performance during the training and validation phases and integrated into an ensemble framework. This diverse combination of models improves predictive accuracy and enhances system reliability in classifying suction and reflux events by detecting underlying patterns. The ensemble of AI models (eAIM) is designed to combine multiple AI models to achieve enhanced performance. It involves model selection, parallel processing, and consensus building. By capitalizing on the unique strengths of each model, the eAIM optimizes decision-making, leading to more precise and reliable pattern recognition (Sagi and Rokach 2018).

The eAIM submodule adheres to the previously established procedure (steps 1–5), with an additional phase dedicated to prediction integration. In this phase, the majority voting technique is employed to aggregate the predictions from the AI models. This method assigns the class with the highest number of votes from the individual models as the final prediction of the eAIM. Although simple, majority voting is an effective strategy for reaching a consensus among the base models. Additionally, combining these three AI models reduces ambiguities caused by potential inference conflicts between individual models, making decision-making more streamlined and reliable.

For the validation metrics (step 5), approximately 90% of the data was randomly sampled from the R1 dataset, encompassing all possible variation states. The evaluation metrics are computed using specific formulas. Accuracy measures the overall correctness of the model by evaluating the proportion of correctly predicted instances, including both

true positives (TP) and true negatives (TN), about the total number of predictions: $(TP + TN) / (TP + TN + FP + FN)$. Precision assesses the model's ability to accurately identify positive instances by calculating the proportion of TP among all cases predicted as positive, including false positives (FP): $TP / (TP + FP)$. The F1 score is a harmonic mean of precision and recall, providing a single metric representing the model's accuracy in predicting positive instances while considering both false positives and false negatives: $TP / (TP + 0.5 * (FP + FN))$.

An additional validation metric for this proposal was derived from the methodology recommended by Maw et al. (2021) and Rocchi et al. (2023) to validate suction events. The study utilized these metrics to assess the model's performance further. Sensitivity (also known as Recall) quantifies the model's ability to accurately identify all actual positive instances by determining the proportion of TP among all the positive cases, including FN. This is calculated as $TP / (TP + FN)$. On the other hand, Specificity (also referred to as the true negative rate) measures the model's effectiveness in correctly identifying negative instances and is given by $TN / (FP + TN)$.

Results

In this study, three AI models—KNN, SVM, and ANN—were implemented for the submodules of the RSD system, focusing on predictive analysis of reflux and suction events. Each model was configured using the Grid Search technique to balance performance and efficiency.

The KNN was configured with the following parameters: `n_neighbors = 5`; `weights = "uniform"`; `algorithm = "auto"`; `leaf_size = 30`; `metric = 'minkowski'`; and `p = 2`.

The choice of `n_neighbors = 5` reflects a widely accepted value in the literature, offering a trade-off between bias and variance to mitigate risks of underfitting and overfitting. A uniform weighting scheme (`weights = "uniform"`) was employed to prevent closer neighbors from disproportionately influencing the decision boundary, thus reducing potential local biases. Setting `algorithm = "auto"` allowed Scikit-Learn to dynamically select the most appropriate algorithm based on the dataset's size and structure, enhancing computational efficiency. The Minkowski distance with `p = 2` (Euclidean distance) was appropriate given the continuous and multidimensional nature of the EEG data.

The SVM model was parameterized: `C = 1.0`; `kernel = "rbf"`; `degree = 3`; `gamma = "scale"`; and `shrinking = True`.

The regularization parameter `C = 1.0` was selected to balance bias and variance. The radial basis function (RBF) kernel was chosen for its effectiveness in handling nonlinear decision boundaries, particularly in complex classification

tasks such as EEG signal processing. The configuration `gamma = "scale"` dynamically adjusts the gamma value based on data variance, promoting adaptive model performance. The shrinking heuristic (`shrinking = True`) was enabled to improve computational efficiency by focusing optimization efforts on the most relevant support vectors.

The ANN model was designed with the following architecture and parameters: Hidden layer: 100 neurons (`hidden_layer_sizes = (100)`); Activation function: ReLU (`activation = "relu"`); Optimizer: Adam (`solver = "adam"`); Regularization: `alpha = 0.0001`; Batch size: `batch_size = "auto"`; Learning rate: `learning_rate_init = 0.001`; and Maximum iterations: 200.

The ReLU activation function was selected for its efficiency and ability to mitigate the vanishing gradient problem, enhancing training stability. Regularization was managed with `alpha = 0.0001`, ensuring moderate model capacity while minimizing overfitting risks. The batch size was automatically adjusted (`batch_size = "auto"`) to balance memory usage and computational performance. An initial learning rate of 0.001 was chosen, as it is well-established in the literature for promoting stable convergence during training. The maximum number of iterations was capped at 200 to ensure efficiency without compromising convergence quality.

These configurations were selected following best practices from the literature on pattern recognition tasks, ensuring that each algorithm was tailored to manage the complexity of pressure wave signals. The following section presents the results of evaluating the RSD system's submodules.

Figure 8 and Fig. 9 display the confusion matrices for each submodule of the RSD system (SA and eAIM {R1, R2}), evaluating the predictions for detecting reflux and suction events, respectively. The SA submodule showed exciting results in suction detection with 99.66% but limitations in accuracy and F1-Score for reflux events. Its accuracy was 80.04% during reflux assessment, indicating increased FP and FN. The F1-Score was 70.4%, reflecting a reduced ability to balance precision and recall. The KNN and SVM models exhibited consistent accuracies exceeding 96% for reflux and suction events with the R1 dataset. The variability of KNN and SVM results suggests more stable behavior than the SA submodule. The ANN stands out due to low variability and consistent RMSE in reflux and suction detection, indicating efficiency in capturing correct event patterns. The RMSE remained low for AI models, with values of 0.07 for the ANN in the R1 dataset, reflecting accurate predictions while minimizing computational errors.

The evaluation metrics—Accuracy, Precision, F1 Score, and RMSE—derived from the confusion matrices shown in Figs. 8 and 9 are summarized in Table 1. The ANN demonstrated the highest accuracy for reflux event detection, achieving 99.39% in Round 1, suggesting its robustness in identifying this specific event. Conversely, the KNN

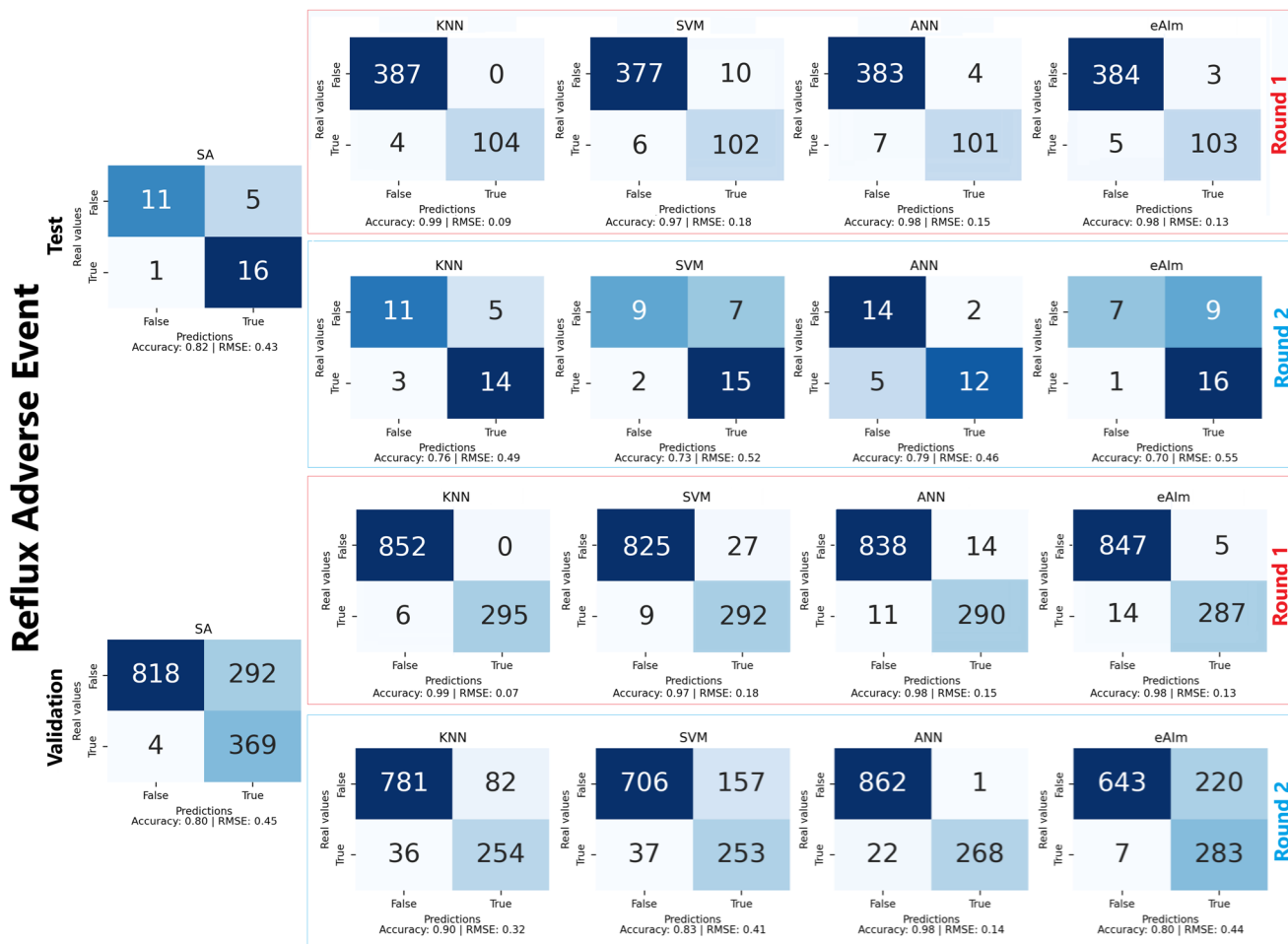


Fig. 8 Confusion matrix comparison for reflux event detection strategies: structured algorithm (SA) and ensemble of AI models: K-nearest neighbors (KNN), support vector machine (SVM), and artificial neural network (ANN)

algorithm, while exhibiting a lower overall accuracy of 81.82%, showed considerable improvement in subsequent rounds, attaining an evaluation score of 89.77% in Round 2, indicating its adaptability with additional training data.

In contrast, the SVM exhibited moderate performance, with accuracy scores fluctuating across rounds, suggesting potential challenges in generalizing across different datasets. Precision metrics revealed that the eAIM achieved an exceptional precision rate of 99% in Round 1 for suction event detection, underscoring its efficacy in minimizing false positives. However, precision values significantly declined in subsequent rounds, highlighting the need for further refinement and training.

The analysis of RMSE indicates that the models performed well in minimizing prediction errors, particularly the ANN, which maintained low RMSE values throughout its evaluation, thereby reinforcing its reliability.

Based on the confusion matrices presented in Fig. 8, sensitivity and specificity were calculated. For reflux detection, the SA submodule achieved a sensitivity of approximately

94% in the test phase and 99% in the validation phase, but with a specificity of around 69% in the test and approximately 74% in the validation. In contrast, for suction detection, the SA submodule demonstrated a sensitivity of roughly 94% in the test phase and 98% in the validation phase, with a perfect specificity of 100% in both phases.

For reflux detection with the R1 dataset, the KNN model achieved a sensitivity of 96% in the test phase and 98% in the validation phase, with a specificity of 100% in both phases. The SVM model recorded a sensitivity of 94%, a specificity of 97% during the test phase, a sensitivity of 97%, and a specificity of 97% during validation. The ANN model demonstrated a sensitivity of 94% and a specificity of 99% in the test phase, with a sensitivity of 96% and a specificity of 98% in the validation phase. Meanwhile, the eAI module achieved a sensitivity of 95% and a specificity of 99% in both test and validation phases.

For the R1 dataset, the results for suction detection were as follows: The KNN model consistently stood out, achieving a sensitivity of 100% and a specificity of 98% in both

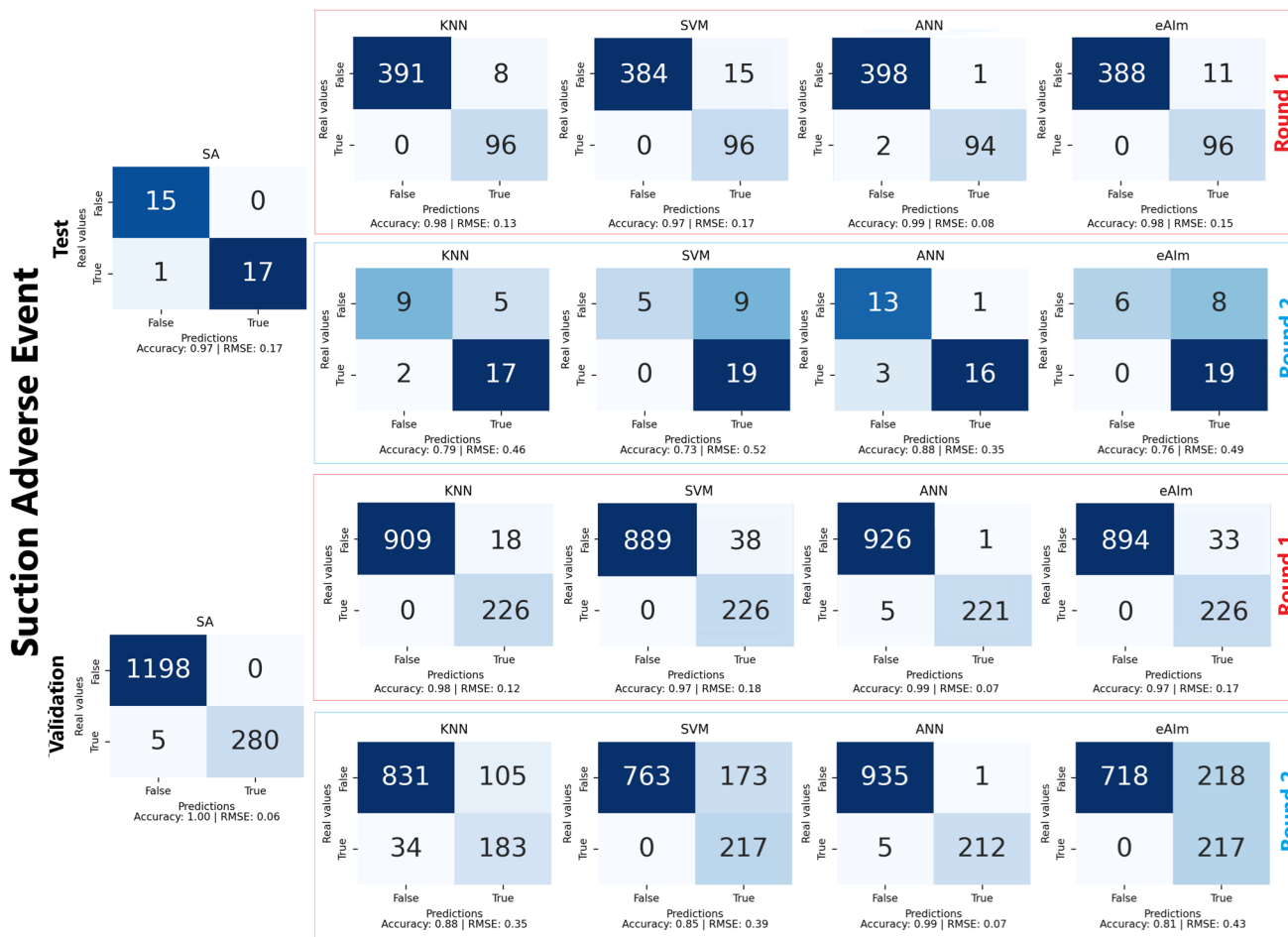


Fig. 9 Confusion matrix comparison for suction event detection strategies: structured algorithm (SA) and ensemble of AI models: K-nearest neighbors (KNN), support vector machine (SVM), and artificial neural network (ANN)

the test and validation phases. The SVM model recorded a sensitivity of 100% and a specificity of 96% in the test and validation phases. The ANN model exhibited a sensitivity of 98% and a specificity of 99% in both phases. In comparison, the eAlm submodule matched the sensitivity of the KNN and SVM models at 100% in the test and validation phases. However, it had a slightly lower specificity of 97% during testing and 96% during validation.

For reflux detection with the R2 dataset, the KNN model achieved a sensitivity of 82% in the test phase and 87% in the validation phase, with a specificity of 69% in the test and 91% during validation. The SVM model recorded a sensitivity of 88% and a specificity of 56% during the test phase, with a sensitivity of 87% and a specificity of 82% during validation. The ANN model demonstrated a sensitivity of 71% and a specificity of 88% in the test phase, with a sensitivity of 92% and a specificity of 100% during validation. Finally, the eAlm submodule achieved a sensitivity of 94%, a specificity of 44% in the test phase, a sensitivity of 98%, and a specificity of 74% during validation.

For the R2 dataset, the results for suction detection were as follows: The KNN model achieved a sensitivity of 64% in the test phase and 84% in the validation phase, with a specificity of 90% during testing and 88% during validation. The SVM model recorded a sensitivity of 100%, a specificity of 36% during testing, and a specificity of 100% and 81% during validation. The ANN model demonstrated a sensitivity of 93% and a specificity of 84% in the test phase, with a sensitivity of 98% and a specificity of 99% during validation. Finally, the eAlm submodule achieved a sensitivity of 100% and a specificity of 43% during the test phase and a sensitivity of 100% with a specificity of 77% during validation.

In the experiments conducted on data classification within the AI-based submodule, as elucidated in Figs. 10 and 11 for reflux and suction detection, respectively, three models (KNN, SVM, RNA) were evaluated across two distinct contexts for two testing scenarios (R1 and R2), considering both the test set and the validation set. The primary metrics reported included each model's mean accuracy, standard deviation, and the highest accuracy.

Table 1 Evaluation metrics (accuracy, precision, F1 score, and RMSE) for reflux and suction event detection strategies: structured algorithm (SA), K-nearest neighbors (KNN), support vector machine (SVM), artificial neural network (ANN), and ensemble of AI models

	Structured Algorithm (SA)	K-nearest neighbors (KNN)	Support vector machine (SVM)	Artificial neural network (ANN)	Ensemble of Artificial Intelligences (eAI)
Reflux event detection					
Accuracy	Test: 81.82% Evaluation: 80.04%	Round 1 Test: 98.38% Evaluation: 98.44%	Round 1 Test: 96.97% Evaluation: 96.7%	Round 1 Test: 99.39% Evaluation: 99.48%	Round 1 Test: 97.78% Evaluation: 97.14%
Precision	Test: 76.2% Evaluation: 55.8%	Round 2 Test: 75.76% Evaluation: 89.77%	Round 2 Test: 72.73% Evaluation: 83.17%	Round 2 Test: 78.79% Evaluation: 98.01%	Round 2 Test: 69.7% Evaluation: 80.31%
F1-Score	Test: 84.2% Evaluation: 70.4%	Round 1 Test: 92.3% Evaluation: 92.6%	Round 1 Test: 86.4% Evaluation: 85.5%	Round 1 Test: 99% Evaluation: 99.5%	Round 1 Test: 89.7% Evaluation: 87.3%
RMSE	Test: 0.43 Evaluation: 0.45	Round 2 Test: 73.6% Evaluation: 75.6%	Round 2 Test: 68.2% Evaluation: 61.7%	Round 2 Test: 85.7% Evaluation: 99.6%	Round 2 Test: 64% Evaluation: 56.3%
Suction event detection					
Accuracy	Test: 96.97% Evaluation: 99.66%	Round 1 Test: 98.38% Evaluation: 98.44%	Round 1 Test: 96.97% Evaluation: 96.7%	Round 1 Test: 99.39% Evaluation: 99.48%	Round 1 Test: 97.78% Evaluation: 97.14%
Precision	Test: 100% Evaluation: 100%	Round 2 Test: 78.79% Evaluation: 87.94%	Round 2 Test: 72.7% Evaluation: 85%	Round 2 Test: 87.88% Evaluation: 99.48%	Round 2 Test: 75.76% Evaluation: 81.09%

Table 1 (continued)

	Structured Algorithm (SA)	K-nearest neighbors (KNN)	Support vector machine (SVM)	Artificial neural network (ANN)	Ensemble of Artificial Intelligences (eAIM)
F1-Score	Test: 97.1% Evaluation: 99.1%	Round 1 Test: 96% Evaluation: 96.3% Round 2 Test: 83% Evaluation: 72.7%	Round 1 Test: 92.6% Evaluation: 92.3% Round 2 Test: 81.1% Evaluation: 70.6%	Round 1 Test: 98.4% Evaluation: 98.6% Round 2 Test: 88.9% Evaluation: 98.6%	Round 1 Test: 94.7% Evaluation: 93.3% Round 2 Test: 82.8% Evaluation: 66.6%
RMSE	Test: 0.17 Evaluation: 0.06	Round 1 Test: 0.13 Evaluation: 0.12 Round 2 Test: 0.46 Evaluation: 0.35	Round 1 Test: 0.17 Evaluation: 0.18 Round 2 Test: 0.52 Evaluation: 0.39	Round 1 Test: 0.08 Evaluation: 0.07 Round 2 Test: 0.35 Evaluation: 0.07	Round 1 Test: 0.15 Evaluation: 0.17 Round 2 Test: 0.49 Evaluation: 0.43

In the R1 dataset during the testing phase for reflux detection, KNN stood out with a mean accuracy of $98.50 \pm 0.53\%$, while SVM achieved $95.57 \pm 1.06\%$, and RNA reached $95.40 \pm 2.52\%$. The highest accuracy was attained by KNN, with 100%, followed by RNA, with 99.19%, and SVM, with 98.79%. In the validation phase, KNN demonstrated even more excellent performance, with a mean accuracy of $98.99 \pm 0.18\%$, followed by SVM at $95.85 \pm 0.49\%$, and RNA at $95.55 \pm 2.40\%$. KNN (100%) achieved the maximum accuracy again, with RNA and SVM maintaining similar performances as observed in the testing phase.

In the R1 dataset during the testing phase for suction detection, the performance of the models was relatively consistent, with KNN achieving a mean accuracy of $97.63 \pm 0.70\%$, followed by SVM at $96.07 \pm 0.72\%$ and RNA at $95.80 \pm 5.20\%$. Regarding peak performance, RNA attained 100% accuracy, surpassing KNN (99.60%), and SVM (98.38%). In the validation phase, even more excellent stability in results was observed. The mean accuracy for KNN was $97.96 \pm 0.15\%$, while SVM presented $96.13 \pm 0.06\%$, and RNA achieved a superior mean of $98.58 \pm 0.33\%$. Once again, RNA demonstrated the best accuracy at 100%, followed by KNN and SVM, retaining their maximum accuracy from the testing phase.

In the R2 dataset during the testing phase for reflux detection, KNN reported a mean of $65.53 \pm 5.95\%$, SVM $73.04 \pm 6.21\%$, and RNA $72.60 \pm 7.12\%$. SVM achieved the highest accuracy of 93.94%, while RNA reached 90.91% and KNN 81.82%. In the validation set, KNN had a mean accuracy of $82.43 \pm 3.47\%$, SVM $77.74 \pm 2.28\%$, and RNA achieved a mean of $88.76 \pm 4.89\%$. The highest accuracies were maintained with values identical to those obtained in the testing phase.

In the R2 dataset during the testing phase for suction detection, the results revealed more significant variation in performance. KNN achieved a mean of $72.52 \pm 6.68\%$, SVM presented $75.07 \pm 6.18\%$, and RNA reached $73.39 \pm 15.23\%$. However, the best accuracy was attained by RNA at 100%, while both KNN and SVM achieved a maximum of 93.94%. In the validation set, RNA significantly outperformed, with a mean accuracy of $98.82 \pm 0.30\%$, considerably exceeding KNN ($81.90 \pm 3.76\%$), and SVM ($76.41 \pm 2.41\%$). RNA also achieved the best accuracy at 100%, confirming its superiority in the validation context.

The results obtained from the eAIM model, as presented in the histogram in Fig. 12, indicate that for the R1 dataset, in the testing phase for reflux detection, the eAIM achieved an accuracy of 98.38% and a RMSE of 0.13; in the validation phase, the accuracy was 98.35% with an RMSE of 0.13. For suction detection in the R1 dataset, the results were an accuracy of 97.78% and an RMSE of 0.15 in the testing phase, while in validation, the accuracy was 97.14% with an RMSE of 0.17. In the R2 dataset, the eAIM obtained an accuracy of 75.75% and an RMSE of 0.50 in the testing phase for suction detection and an accuracy of 81.09% with an RMSE of 0.43 in validation. For reflux detection in the R2 dataset, the testing phase presented an accuracy of 69.69% and an RMSE of 0.55, while in validation, the accuracy was 80.31% with an RMSE of 0.44.

Discussion

A redundancy RSD system enhances the reliability of event classification. Furthermore, each RSD submodule should possess distinct advantages to address the extensive

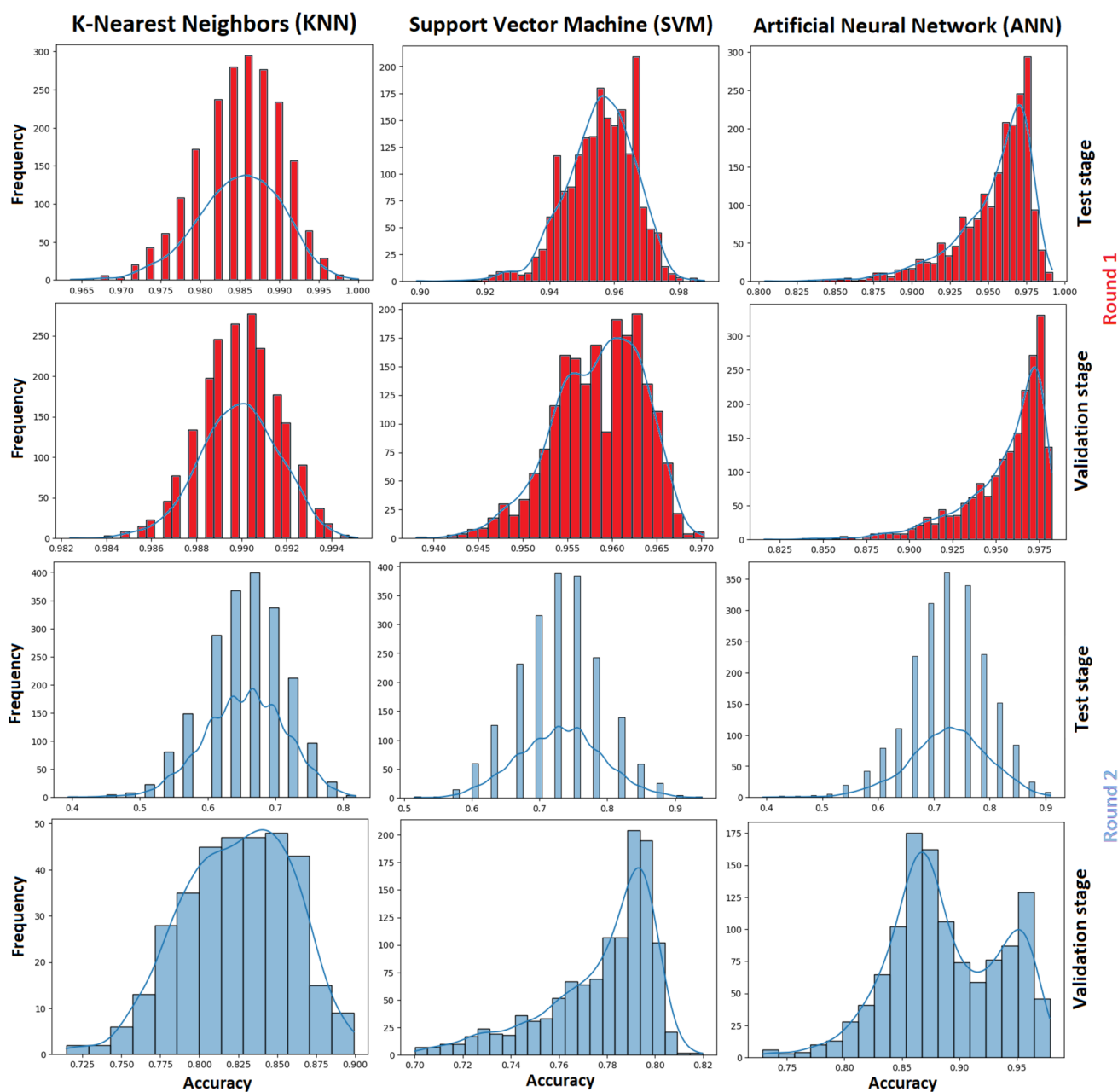


Fig. 10 Histogram chart comparing the performance of artificial intelligence models in reflux prediction: K-nearest neighbors (KNN), support vector machine (SVM), and artificial neural network (ANN)

diversity of functionality and criticality encountered in clinical applications.

The strategy based on the SA algorithm, implemented as a submodule within the RSD system, has shown promising results in detecting reflux and suction events. Although the obtained metrics are not optimal, when considering only the training with the R2 dataset, the accuracy achieved for suction event detection was the highest (99.66%). Conversely, the accuracy for reflux event detection was the lowest (80.04%). Despite this, the overall results are still

favorable and comparable to those of more complex models that require significant computational power. Moreover, the SA submodule is highly advantageous due to its ease of implementation in microcontrollers, which are widely used in commercial LVAD controllers (Santos et al. 2024).

Due to the relatively poorer metrics associated with the SA submodule, an exciting approach could involve using it as an initial indicator that a malfunction may occur. Subsequent confirmation of the event could be achieved through the eIAM submodule of the RSD system. Following this

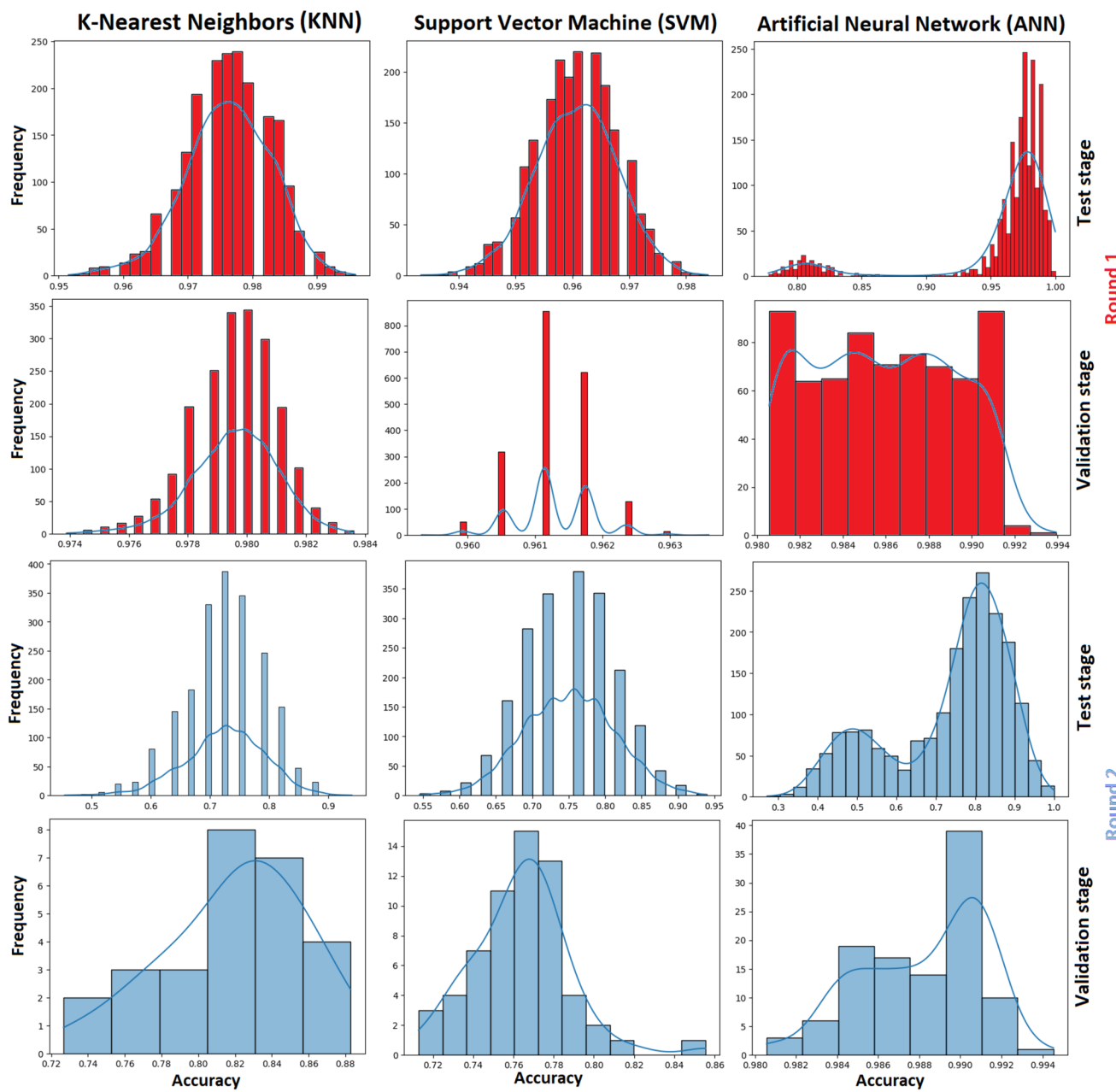


Fig. 11 Histogram chart comparing the performance of artificial intelligence models in suction prediction: K-nearest neighbors (KNN), support vector machine (SVM), and artificial neural network (ANN)

confirmation, the PC-LVAD should mitigate the event (Ferreira et al. 2008; Sadatih et al. 2021), and the physician should be notified for further investigation. In this context, a complementary approach to the RSD system may involve a submodule based on the suction detector proposed by Ferreira et al. (2008), which employs a discriminant analysis model to classify pump flow patterns into three categories accurately: no suction, moderate suction, and severe suction. The generated discriminant scores are inputs for a fuzzy logic controller, which adjusts the pump

speed to maintain proper flow and pressure perfusion to the patient.

The fuzzy logic system exhibits a duality: while its logical framework is relatively straightforward, its implementation can be complex. However, we have successfully migrated a PC-LVAD with fuzzy logic, developed on a personal computer, to an embedded system based on a field-programmable gate array (FPGA) and real-time operating system (RTOS) (Santos et al. 2024). This additional submodule can operate in a cascade check after the SA submodule, which identifies

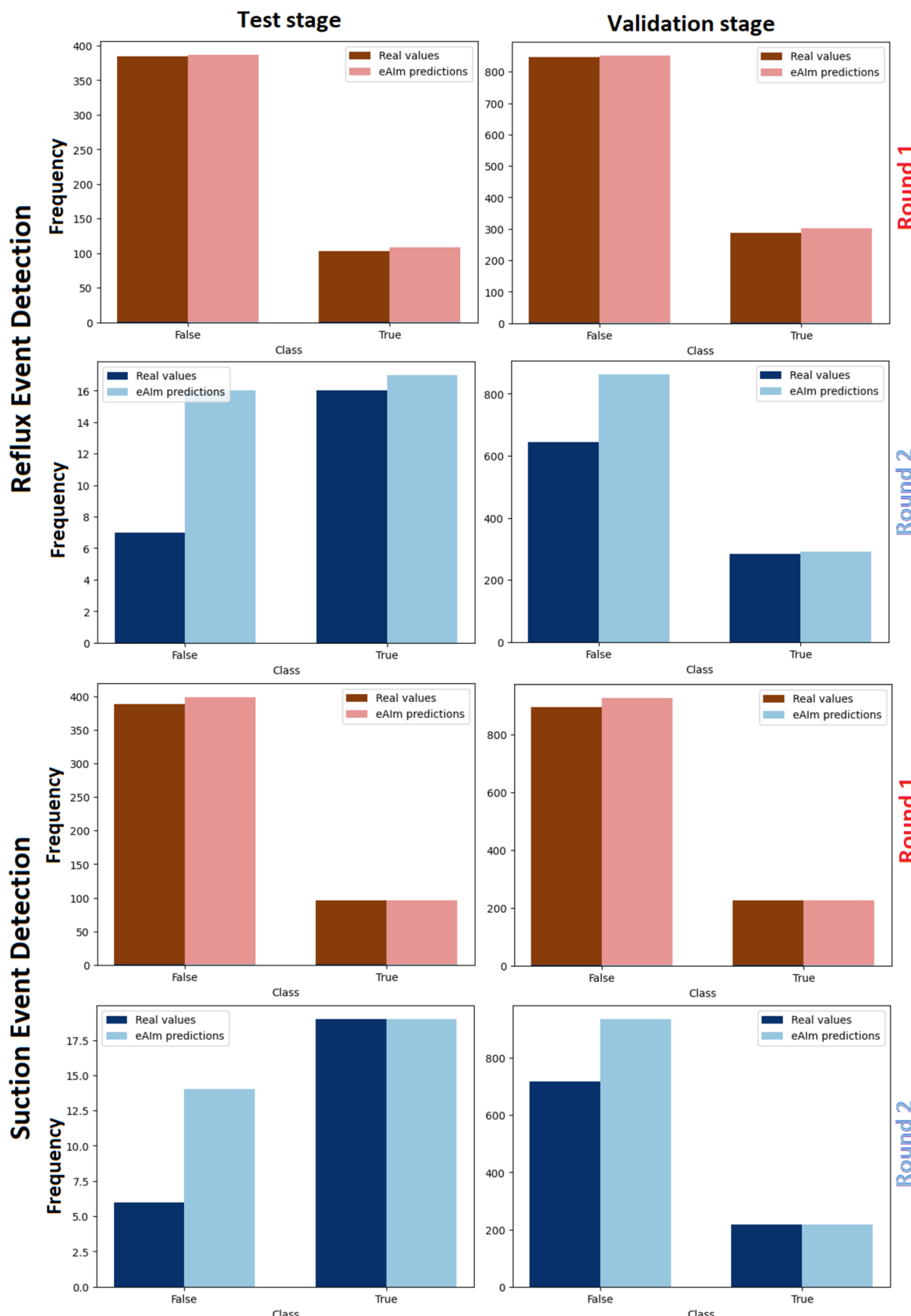


Fig. 12 Histogram showing a comparison of predictions made by the ensemble of K-nearest neighbors (KNN), support vector machine (SVM), and artificial neural network (ANN) models during the reflux and suction prediction rounds on the dataset

the occurrence of any adverse events related to suction or reflux before confirmation via the eAIm submodule.

The study by Sadatieh et al. (2021) utilizes extremum-seeking control (ESC) to regulate the speed of LVADs, improving performance by maximizing cardiac output and preventing suction events without the need for a mathematically defined objective function. In this proposal, the ESC controller demonstrated in silico effectiveness across various physiological conditions, ranging from rest to intense physical activity, and maintained satisfactory performance even with noisy measurements. The controller rapidly adjusts the pump speed when necessary to prevent suction.

However, the ESC approach has been widely criticized due to several significant limitations (Krstić, 2000): (i) Slow convergence, particularly in complex or noisy systems, and its sensitivity to fluctuations; (ii) improper parameter tuning may lead to oscillations or instability, and performance is highly dependent on precise adjustment, making the tuning process labor-intensive; (iii) ESC faces substantial difficulty in handling multiple local extrema and systems with fast dynamics, and (iv) it lacks formal optimization guarantees and may be computationally complex to implement.

A complementary approach could involve using two or more controllers operating in parallel. In this configuration, a PC-LVAD system could employ a multi-objective strategy (Petrou et al. 2018; Leão et al. 2020), integrating an RSD-based controller while an ESC operates simultaneously. The controller that achieves optimal performance in a given situation without introducing risks would be selected to act directly on the LVAD pump, ensuring optimal support and recovery for the patient.

When comparing the outcomes derived from the R1 and R2 datasets, a distinct disparity in model performance for detecting suction and reflux is evident, particularly in sensitivity and specificity metrics. The R1 dataset consistently produced superior results, characterized by enhanced sensitivity and specificity across all models, whereas the R2 dataset exhibited a marked reduction in performance, notably in terms of specificity.

The performance superiority of the R1 dataset was consistently observed across all models, with high levels of sensitivity and specificity for both suction and reflux detection tasks. These findings strongly indicate that R1 is the more suitable dataset for training and validating models designed to accurately differentiate the events under investigation. The models showed a reliable capability to detect suction and reflux, with minimal occurrences of false positives and false negatives.

In contrast, the R2 dataset posed significant challenges, particularly concerning specificity, with specific models—such as SVM and eAIm—demonstrating increased false-positive rates. Nevertheless, the ANN model maintained relatively stable performance, especially during the

validation phase. In conclusion, the R1 dataset provided more robust and consistent outcomes. In contrast, the R2 dataset introduced a significant reduction in performance, particularly in reflux detection, underscoring the necessity for further optimization when employing the R2 dataset for these detection tasks.

The expectation was superior performance from the R1 dataset, as it encompasses all simulation scenarios. Indeed, its metrics yielded exciting results. However, the simplified dataset (R2) performance did not lag significantly behind. Specifically, in reflux conditions, the accuracy of the eAIm was 97.14% for R1 and 80.31% for R2, while in suction conditions, it was 97.14% for R1 and 81.09% for R2. This indicates that, in clinical practice, it may be feasible to utilize AI models specialized in detecting AEs related to suction and reflux. Such models could be based on patient specificity through a training approach similar to that used for the R2 dataset, incorporating information derived from both in silico and *in vitro* simulations.

The KNN model emerged as the most effective algorithm for detecting reflux and suction events, achieving an accuracy of 97% for suction detection and 98.38% for reflux detection in Round 1. This performance was corroborated by evaluation metrics of 99.66% for suction and 98.44% for reflux, respectively. The ANN followed closely, demonstrating accuracies of 99.39% for reflux detection and 97% for suction detection, with corresponding evaluations of 99.48% and 96.7%, respectively. While the ANN exhibited robust performance in reflux detection, its marginally lower accuracy in suction detection suggests potential avenues for optimization regarding its configuration or training parameters. The SVM also delivered competitive results, achieving accuracies of 97% for suction detection and 98.38% for reflux detection, indicating its effectiveness in specific scenarios; however, its performance exhibited variability across different evaluation rounds.

These results can be attributed to the inherent characteristics of the AI models and the nature of the data used. The KNN algorithm is a supervised learning method that classifies new data based on similarity to nearby examples in the feature space. It is effective for data with a clear local structure and balanced distribution. However, its performance may deteriorate with high-dimensional data or when there is significant overlap between classes. Conversely, ANNs are adept at identifying complex patterns in nonlinear data, although their effectiveness depends on the quality and quantity of the data and the selection of parameters. SVMs are proficient in separating linear classes but may struggle with nonlinear or outlier data.

The comprehensive analysis of the results indicates a clear superiority of the ANN model in the validation scenario, particularly within the R2 context, where it achieved the highest accuracy across all cases. However, the KNN

algorithm demonstrated consistent effectiveness in the R1 context, especially in the Reflux task, whereas the SVM exhibited more variable performance, occasionally standing out in terms of superior accuracy. The eAIM model also demonstrated satisfactory precision, albeit with variations contingent on the scenario and the evaluated data. The eAIM may be highly recommended to optimize outcomes in scenarios where accuracy and reliability are critical.

Maw et al. (2021) presented a development of suction detection algorithms and highlighted that a unique feature classifier achieved a sensitivity of 100% and a specificity of 95.5%. In contrast, an ensemble classifier exhibited a reduced sensitivity of 92.5% due to overfitting while maintaining a specificity of 100%. In our proposal, the eAIM submodule demonstrates improved results, achieving a perfect sensitivity of 100% across both datasets and a specificity of 96% on the R1 and 100% on the R2 datasets. Integrating these AI models into an ensemble method provides a comprehensive approach to pattern detection in pressure wave readings, addressing the diverse needs of patients across various scenarios. Training the ensemble program is computationally intensive, requiring over 1 h; however, once trained and saved as a model file, it operates in real-time, demanding minimal storage and processing resources.

To generate a pressure wave in the inlet cannula of the cfLVAD, the heart must retain some contractile function to propel the fluid and create a measurable pressure wave detectable by sensors. Furthermore, a susceptible and calibrated sensor is required for monitoring purposes. The application of differential pressure, measured between the inlet and outlet, is pivotal in enhancing the inference accuracy of AI models in cardiovascular devices. While inlet pressure measurement alone can result in sawtooth-like waveforms, differential pressure offers a more comprehensive depiction of system variations, facilitating a detailed and precise analysis. Although there is potential for increased drift and noise over time, advanced AI interpretative capabilities can mitigate these effects, maintaining analytical precision. However, this hypothesis necessitates validation through rigorous experiments to confirm the model's efficacy under varying noise and drift conditions.

The peaks and troughs of the pressure waveform are subject to significant changes due to variations in preload and afterload characteristics, reflecting the complex dynamics of the cardiovascular system. Unlike traditional methods that focus on isolated parameters, an AI-based system analyzes the entire composition of the pressure waveform. This encompasses subtle patterns and interrelations among multiple factors, potentially enhancing precision in detecting AEs such as ventricular suction. Nonetheless, the effectiveness of this AI-based approach must be verified through rigorous experiments to confirm its superiority over conventional methods.

Our findings are derived from in silico studies employing a computational simulator to explore nonlinear responses. A more conservative approach would be to regard the results as merely indicative of the potential of the proposed methods, given the anticipated reduction in accuracy in practical applications. Nonetheless, the high accuracy and low RMSE values obtained in the submodules tested suggest that the patterns identified can readily be detected in computational simulations. In vitro studies are necessary to validate the obtained metrics. In this context, Ochsner et al. (2013) developed a suction module for a hybrid mock circulation, in which suction is simulated via software and a minimum Pindex value is used to assess suction. Experimental results demonstrate that suction can be emulated as desired; however, the figures do not precisely match those from in vivo experiments. To improve this, the work of Rocchi et al. (2023) employed physical simulation of suction using a latex tube that mimics the ventricular apex, and the validation included induction of suction under these specific conditions and subsequent comparison with clinical data collected from patients with LVAD. In the Rocchi et al. (2023) study, sensitivity and specificity results were 90% and 97.5%, respectively. The RSD system for detecting suction in silico demonstrated significant performance metrics during its validation phase. Specifically, the SA submodule achieved a sensitivity of approximately 98% and a specificity of 100%. In the analysis of the R1 dataset, the eAIM submodule exhibited a perfect sensitivity of 100% and a specificity of 96%. Similarly, for the R2 dataset, the eAIM submodule maintained a sensitivity of 100%, although its specificity was recorded at 77% during the validation process. This suggests that not only are the results obtained satisfactory but also that the variation of the scenarios evaluated in silico can approach the variation obtained in the in vitro study.

Conclusion

The study presents a novel approach for evaluating an RSD system applied to a cfLVAD using inlet and outlet pressure measurements. Two submodules were examined using a structured algorithm and ensemble AI to effectively detect reflux and suction events. This approach is unprecedented in the literature, as it identifies new waveform patterns for classifying suction and reflux events. It represents the first application of AI for integrating both adverse events, with enhanced result robustness achieved through combining multiple AI models. RSD system demonstrated excellent results, suggesting their viability for application to PC-LVADs. The good results of the in silico study indicate the potential of the approach described, as a reduction in accuracy is anticipated in practical applications. A critical point

for future research is whether the developed systems can adequately detect suction and reflux in real time.

Acknowledgements The authors would like to thank the financial support of São Paulo State Foundation (FAPESP, Grant 2012/50283-6), FINEP (Grant 01.14.0177.00) and National Council for Research and Development (CNPq).

Funding São Paulo State Foundation (FAPESP, Grant 2012/50283-6); FINEP (Grant 01.14.0177.00); and University of São Paulo (USP).

Data availability Not applicable.

Code availability Not applicable.

Declarations

Ethics approval and consent to participate Not applicable.

Conflicts of interest The authors declare no conflict of interest.

References

- Abiodun OI, Jantan A, Omolara AE, Dada KV, Mohamed NA, Arshad H. State-of-the-art in artificial neural network applications: a survey. *Heliyon*. 2018;4(11):e00938.
- Bouchez S, Erb J, Foubert L, Mauermann E. Pressure-volume loops for reviewing right ventricular physiology and failure in the context of left ventricular assist device implantation. In: Seminars in Cardiothoracic and Vascular Anesthesia. 2023;27(4):283–291. Sage CA: Los Angeles, CA: SAGE Publications.
- Bronicki RA, Tume SC, Flores S, Loomba RS, Borges NM, Penny DJ, Burkhoff D. The cardiovascular system in severe sepsis: Insight from a cardiovascular simulator. *Pediatr Crit Care Med*. 2022;23(6):464–72.
- Cervantes J, Garcia-Lamont F, Rodríguez-Mazahua L, Lopez A. A comprehensive survey on support vector machine classification: applications, challenges, and trends. *Neurocomputing*. 2020;408:189–215.
- Choi S, Boston JR, Antaki JF. Hemodynamic controller for left ventricular assist device based on pulsatility ratio. *Artif Organs*. 2007;31(2):114–25.
- Dahl OJ, Dijkstra EW, Hoare CAR. Structured programming. GBR: Academic Press Ltd.; 1972. <https://dl.acm.org/doi/10.5555/1243380>
- de Sousa MADA. The shift of artificial intelligence research from academia to industry: implications and possible future directions. *Ai Soc*. 2024;1–10. <https://doi.org/10.1007/s00146-024-01924-0>.
- Deniz E, Hanke JS, Schwick F, Rojas-Hernandez SV, Dogan G, Feldmann C, ... Schmitto JD. First experience with the HeartAssist5® left ventricular assist device. *Thorac Cardiovasc Surg*. 2017;65(S 01), OP223.
- Doshi D, Burkhoff D. Cardiovascular simulation of heart failure pathophysiology and therapeutics. *J Cardiac Fail*. 2016;22(4):303–11.
- Dual SA, Zambrano BL, Sündermann S, Cesarovic N, Kron M, Magkoutas K, ... Daners MS. Continuous heart volume monitoring by fully implantable soft strain sensor. *Adv Healthcare Mater*. 2020;9(19):2000855.
- Ferreira A, Boston JR, Antaki JF. A control system for rotary blood pumps based on suction detection. *IEEE Trans Biomed Eng*. 2008;56(3):656–65.
- Fetanat M, Stevens M, Hayward C, Lovell NH. Using a real-time deep convolutional neural network, a sensorless control system for an implantable heart pump. *IEEE Trans Biomed Eng*. 2021;68(10):3029–38.
- Goodman D, Stulak J, Rosenbaum AN. Left ventricular assist devices: a historical perspective at the intersection of medicine and engineering. *Artif Organs*. 2022;46(12):2343–60.
- Horvath DJ, Kuban BD, Golding, LA. U.S. Patent No. 10,077,777. Washington, DC: U.S. Patent and Trademark Office. 2018.
- Ishii, K., Saito, I., Isayama, T., Nakagawa, H., Emiko, N., Ono, T., ... & Abe, Y. (2012). Development of normal-suction boundary control method based on inflow cannula pressure waveform for the undulation pump ventricular assist device. *Artificial Organs*, 36(9), 812–816.
- Jorde UP, Saeed O, Koehl D, Morris AA, Wood KL, Meyer DM, ... Vega JD. The society of thoracic surgeons interagency registry for mechanically assisted circulatory support 2023 Annual Report: focus on magnetically levitated devices. *Ann Thorac Surg*. 2023. <https://doi.org/10.1016/j.athoracsur.2023.11.004>.
- Krstić M. Performance improvement and limitations in extremum seeking control. *Syst Control Lett*. 2000;39(5):313–26.
- Leao T, Utiyama B, Fonseca J, Bock E, Andrade A. In vitro evaluation of multi-objective physiological control of the centrifugal blood pump. *Artif Organs*. 2020;44(8):785–96.
- Lilly LS. Braunwald's heart disease review and assessment E-Book: a companion to Braunwald's heart disease. Elsevier Health Science. 2022. <https://books.google.com.br/books?id=ZE2BEAAQBAJ>
- Magkoutas K, Rossato LN, Heim M, Daners MS. Genetic algorithm-based optimization framework for control parameters of ventricular assist devices. *Biomed Signal Process Control*. 2023;85:104788.
- Mantha A, Lee RO, Wolfson AM. Patient selection for heart transplant: balancing risk. *Curr Opin Organ Transplant*. 2022;27(1):36–44.
- Maw M, Gross C, Schlöglhofer T, Dimitrov K, Zimpfer D, Moscato F, Schima H. Development of suction detection algorithms for a left ventricular assist device from patient data. *Biomed Signal Process Control*. 2021;69:102910.
- Melo TR, Neto JS, Cestari IA, Lima AM. Feedback controller for restoring the basal hemodynamic condition with a rotary blood pump used as left ventricular assist device. *Biomed Signal Process Control*. 2020;62:102136.
- Ochsner G, Amacher R, Daners MS. Emulation of ventricular suction in a hybrid mock circulation. In: 2013 European Control Conference (ECC). Zurich, Switzerland: IEEE; 2013. pp. 3108–3112. <https://ieeexplore.ieee.org/abstract/document/6669530>
- Pauls JP, Stevens MC, Bartnikowski N, Fraser JF, Gregory SD, Tansley G. Evaluation of physiological control systems for rotary left ventricular assist devices: an in-vitro study. *Ann Biomed Eng*. 2016;44:2377–87.
- Peev MP, Salerno CT. HeartMate 3. In: Mechanical Circulatory Support. Cham: Springer International Publishing; 2023. p. 1–18.
- Petersdorff-Campen KV, Dupuch MA, Magkoutas K, Meboldt M, Hierold C, Daners MS. Pressure and bernoulli-based flow measurement via a tapered inflow VAD cannula. *IEEE Trans Biomed Eng*. 2021;69(5):1620–9.
- Petrou A, Ochsner G, Amacher R, Pergantis P, Rebholz M, Meboldt M, SchmidDaners M. A physiological controller for turbodynamic ventricular assist devices based on left ventricular systolic pressure. *Artif Organs*. 2016;40(9):842–55.
- Petrou A, Monn M, Meboldt M, SchmidDaners M. A novel multi-objective physiological control system for rotary left ventricular assist devices. *Ann Biomed Eng*. 2017;45(12):2899–910.
- Petrou A, Lee J, Dual S, Ochsner G, Meboldt M, SchmidDaners M. Standardized comparison of selected physiological controllers for rotary blood pumps: in vitro study. *Artif Organs*. 2018;42(3):E29–42.
- Rocchi M, Gross C, Moscato F, Schlöglhofer T, Meyns B, Fresiello L. An in vitro model to study suction events by a

- ventricular assist device: validation with clinical data. *Front Physiol.* 2023;14:1155032.
- Sadatieh S, Dehghani M, Mohammadi M, Boostani R. Extremum-seeking control of left ventricular assist device to maximize the cardiac output and prevent suction. *Chaos, Solitons Fractals.* 2021;148:111013.
- Sagi O, Rokach L. Ensemble learning: a survey. *Wiley Interdiscip Rev: Data Mining Knowl Disc.* 2018;8(4):e1249.
- Santos B, Cestari I. A Multi-objective physiological control for continuous flow left ventricular assist devices: comparison of estimator versus sensor-based feedback. In 2023 45th Annual International Conference of the IEEE Engineering in Medicine & Biology Society (EMBC) 2023;1–5. IEEE. <https://doi.org/10.1109/EMBC40787.2023.10340974>.
- Santos B, Cestari I. Development of a computational simulator of the physiological control of ventricular assist devices (VADs). In: Marques, J.L.B., Rodrigues, C.R., Suzuki, D.O.H., Marino Neto, J., García Ojeda, R. (eds) IX Latin American Congress on Biomedical Engineering and XXVIII Brazilian Congress on Biomedical Engineering. CLAIB/CBEB 2022 2022. IFMBE Proceedings. 2024;98. Springer, Cham. https://doi.org/10.1007/978-3-031-49401-7_47.
- Santos B, Leão T. Control systems. In Bioengineering and Biomaterials in Ventricular Assist Devices (pp. 75–109). CRC Press. <https://doi.org/10.1201/9781003138358-5>.
- Santos B, Barboza M, Leão T, Santos D, Andrade A, Bock E. Intelligent embedded system for physiological control of ventricular assist devices in health 4.0 Background. *Int J Adv Med Biotechnol - IJAMB*. 2023;5(2). <https://doi.org/10.52466/ijamb.v5i2.112>.
- Santos BJ, Leão TF, Silva MB, da Silva ED, Bock EGP. Embedded cyber-physical system for physiological control of ventricular assist devices. *J Electron Electr Eng* 2024;148–165. <https://doi.org/10.37256/jeee.3120244199>.
- Sayer G, Jeevanandam V, Ota T, Uriel N. Invasive hemodynamic echocardiographic ramp test in the HeartAssist5 LVAD: insights into device performance. *ASAIO J.* 2017;63(2):e10–2.
- Stephens AF, Gregory SD, Burrell AJ, Marasco S, Stub D, Salamonsen RF. Physiological principles of Starling-like control of rotary ventricular assist devices. *Expert Rev Med Devices.* 2020;17(11):1169–82.
- Stevens MC, Stephens A, AlOmari AHH, Moscato F. Physiological control. In Mechanical Circulatory and Respiratory Support (pp. 627–657). Academic Press. <https://doi.org/10.1016/B978-0-12-810491-0.00020-5>.
- Tchatchaleishvili V, Luc JG, Cohan CM, Phan K, Hübbert L, Day SW, Massey HT. Clinical implications of physiologic flow adjustment in continuous-flow left ventricular assist devices. *ASAIO J.* 2017;63(3):241–50.
- Torres DS, Mazzetto M, Cestari IA. A novel automated simulator of pediatric systemic circulation: design and applications. *Biomed Signal Process Control.* 2021;70:102926.
- Vollkron M, Schima H, Huber L, Benkowski R, Morello G, Wieselthaler G. Development of a reliable automatic speed control system for rotary blood pumps. *J Heart Lung Transplant.* 2005;24(11):1878–85.
- Wang Y, Koenig SC, Slaughter MS, Giridharan GA. Rotary blood pump control strategy for preventing left ventricular suction. *ASAIO J.* 2015;61(1):21–30.
- Wu Y. Adaptive physiological speed/flow control of rotary blood pumps in permanent implantation using intrinsic pump parameters. *ASAIO J.* 2009;55(4):335–9.
- Zhang Z. Introduction to machine learning: k-nearest neighbors. *Ann Transl Med.* 2016;4(11):218.

Publisher's Note Springer Nature remains neutral with regard to jurisdictional claims in published maps and institutional affiliations.

Springer Nature or its licensor (e.g. a society or other partner) holds exclusive rights to this article under a publishing agreement with the author(s) or other rightsholder(s); author self-archiving of the accepted manuscript version of this article is solely governed by the terms of such publishing agreement and applicable law.